

# **Petrographic Analysis of Concrete Core Samples from Saltstone Disposal Unit #6 at the Savannah River Site, Aiken, SC**

Robert D. Moser, E. Rae Gore, and Kyle L. Klaus

March 2016



---

## **Executive Summary:**

This study examined five concrete cores provided to the ERDC by the U.S. Department of Energy Savannah River Site from its Saltstone Disposal Unit #6 facility (SDU6). The five cores, which were logged in as CMB No. 160051-1 to 160051-5 which were removed from three different floor placement locations in the structure were subjected to an in-depth analysis consisting of visual and petrographic examination, electron microscopy, pH measurements, elemental mapping, and air void analysis. The results of the study indicated through depth cracks in the slabs that appeared to be driven by shrinkage. Additional analysis identified that smaller cracks less than 0.1 mm in width possible occurring at early ages in the concrete had largely self healed while larger through depth cracks with widths greater than 0.1 mm and in many cases greater than 0.5 mm remained. Many of these large cracks had been successfully infilled with epoxy with the exception of large voids which intersected the cracks. Cracks often intersected coarse aggregates, indicating that the cracks likely occurred at later ages when the concrete strength was high. No vertical displacement was observed between adjacent crack faces. pH indicator solution measurements made using optical microscopy indicated that high pH remains within the concrete even adjacent to cracks. The near surface concrete has reduced pH to depths of up to 2 mm caused by exposure to acidic water and carbonation. The internal composition of the concrete and the paste microstructure were as anticipated based on the mixture proportion used and constituents. The concrete appears to contain all materials specified, at the correct proportions, and meeting specified concrete property requirements such as air content. Overall, the concrete appears to be of competent quality with the exception of cracking. The cracking is likely driven by shrinkage, both drying and autogenous, combined with restraint conditions associated with the sequence of floor slab placements. This conclusion on driving mechanisms for cracking is based on petrographic observations combined with knowledge of the concrete mixture proportion used at SDU6. Crack formation and growth driven by shrinkage has likely ceased and existing cracks are passive.

# Table of Contents

<b>Executive Summary:</b> .....	<b>i</b>
<b>Preface</b> .....	<b>iii</b>
<b>1 Introduction</b> .....	<b>1</b>
<b>2 Scope</b> .....	<b>4</b>
<b>3 Experimental Methods</b> .....	<b>5</b>
3.1 Optical Microscopy.....	5
3.2 Scanning Electron Microscopy and Elemental Mapping.....	5
3.3 pH Indicator Mapping with Optical Microscopy .....	6
3.4 Air Void Analysis .....	6
<b>4 Core Sample #1</b> .....	<b>7</b>
4.1 Optical Microscopy.....	8
4.2 pH Indicator Solution and Microscopy.....	13
4.3 Electron Microscopy and Elemental Mapping .....	14
4.4 Air Void Analysis .....	17
<b>5 Core Sample #2</b> .....	<b>18</b>
5.1 Optical Microscopy.....	19
<b>6 Core Sample #3</b> .....	<b>21</b>
6.1 Optical Microscopy.....	22
6.2 pH Indicator Solution and Microscopy.....	26
6.3 Electron Microscopy and Elemental Mapping .....	28
6.4 Air Void Analysis .....	32
<b>7 Core Sample #4</b> .....	<b>33</b>
7.1 Optical Microscopy .....	34
<b>8 Core Sample #5</b> .....	<b>38</b>
8.1 Optical Microscopy.....	39
8.2 pH Indicator Solution and Microscopy.....	43
8.3 Electron Microscopy and Elemental Mapping .....	45
8.4 Air Void Analysis .....	47
<b>9 Summary and Conclusions</b> .....	<b>48</b>
<b>Contact Information</b> .....	<b>52</b>

## **Preface**

This study was conducted in support of the U.S. Department of Energy Savannah River Site, Aiken, SC, to assess materials and cracking and the Saltstone Disposal Unit #6 Facility. The technical monitor was Dr. Charles A. Weiss Jr. of the U.S. Army Engineer Research and Development (ERDC).

The work was performed by the Concrete and Materials Branch (GMC), of the Engineering Systems and Materials Division (GM), US Army Engineer Research and Development Center (ERDC), Geotechnical and Structures Laboratory (ERDC-GSL). At the time of publication, Christopher M. Moore was Chief, CEERD-GMC; Dr. Gordon W. McMahon was Chief, CEERD-GM. The Deputy Director of ERDC-GSL was Dr. William P. Grogan and the Director was Mr. Bartley P. Durst.

COL Bryan Green was the Commander of ERDC and Dr. Jeffery P. Holland was the Director.

# 1 Introduction

The Geotechnical and Structures Laboratory of the ERDC was requested to perform an analysis on concrete core samples extracted from five locations in the recently-constructed Saltstone Disposal Unit #6 (SDU6) and the Department of Energy Savannah River Site near Aiken, SC. The SDU6 facility consists of a 30 million gallon tank constructed using specialized concrete material developed to be durable from the structure's desired service life considering environmental exposures and the grout material it will contain. The concrete consists of a quaternary blend of portland cement, fly ash, slag, and silica fume with a maximum water-to-cementitious materials ratio of 0.38. The concrete mixture proportion used is provided in Table 1 below.

**Table 1. Mixture proportion for concrete used in SDU6 construction.**

Material	Type	Mass (lb/yd <sup>3</sup> except as noted)	Mass (kg/m <sup>3</sup> except as noted)
Cement	Lehigh Type V	213	126
Fly Ash	Southeastern Class F	163	97
Slag	Holcim Grade 100	284	168
Silica Fume	WR Grace Force 10,000	50	30
Fine Aggregate	Dixiana #33	991	588
Coarse Aggregate	Dogwood #67	1850	1098
Air Entrainer	Darex II	3.91 oz	116 mL
Water Reducer	WRDA 35	42.6 oz.	1260 mL
High-Range Water Reducer	ADVA 380	34.1 oz.	1008 mL
Water	Potable	269	160

The structure consists of a concrete floor, wall panels, and a roof structure with supporting columns internal to the tank. The floor was placed in ten different sections starting on 2 June 2014 and completing on 25 September 2014. Following the floor placements, walls and columns were constructed and then the roof structure was placed. Details of the floor placement are provided in Figure 1 below. Following the floor placements, cracking was noted. Different types of cracking were noted at different ages following the concrete placement. Minor crazing cracks were noted at approximately 2 days after the placement, followed by larger cracks were reported to have occurred weeks after the placement. An example of cracks

observed is shown in Figure 2. Map cracking was observed throughout the slabs but appeared to be more severe in locations with additional restraint. This was especially true for slabs placed later during construction such as Floor 8 which was the final placement which was restrained on two edges (location of Core #5).

Figure 1. Floor placement layout and sequence placement noted by dates on floor slabs. Location of five cores sent to ERDC for analysis are also noted.

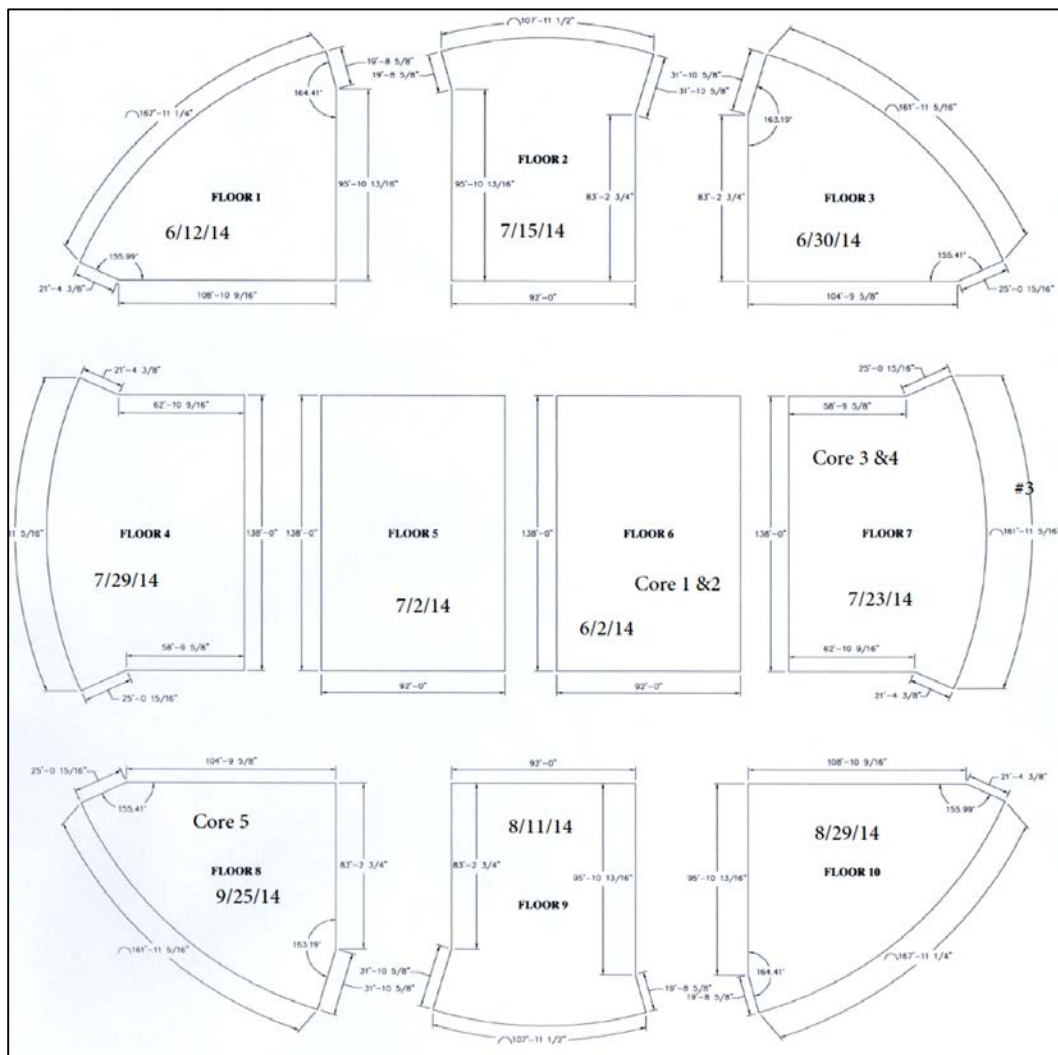
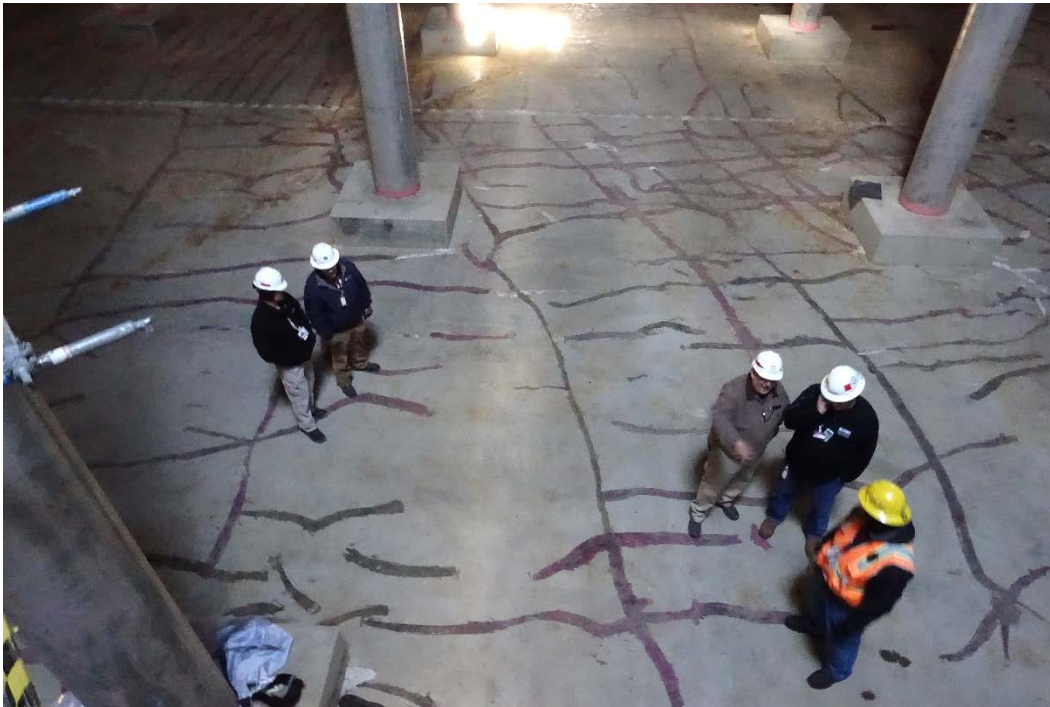


Figure 2. Photograph taken from scaffolding above floor showing locations of cracks. Map cracking observed throughout the slabs highlighted here in purple due to epoxy which was gravity fed into cracks. Two columns can be observed at the top of the picture as well as a construction joint line which has been pressure injected with epoxy.



Due to the observed cracking, the ERDC was requested to conduct a petrographic analysis of the concrete. Cores were extracted from five locations in the floor of the SDU6 tank. These cores were subjected to an in-depth analysis consisting of optical and electron microscopy, X-ray microanalysis, and other types of testing to diagnose the cause of the cracking. In addition, information on the concrete mix design, construction practices, and concrete placement sequence were also provided to the ERDC for consideration.

The following sections describe the scope of the analysis performed by the ERDC, the results of the analysis, and conclusions and recommendations of the study.

## 2 Scope

Five concrete cores were provided to the ERDC for analysis from the locations identified in Figure 1. Two cores were extracted from floor 6 and floor 7 while one core was extracted from floor 8. Table 2 lists the cores received with the original sample identifier, corresponding floor placement number, CMB serial number, and testing performed for each core. The cores were all logged in under CMB serial number 160051. All five cores were analyzed using optical microscopy to quantify the depth and width of cracks. Additional analysis was performed on cores 1, 3, and 5 as these were produced from concrete from each floor placement. This analysis consisted of electron microscopy, elemental mapping, pH indicator measurements, and air void analysis. ERDC was tasked with analyzing the depth and size of cracks, determining the effectiveness of epoxy sealing of cracks, identifying conformance of microstructure with anticipated composition based on the mixture proportion, and quantifying the air content of the concrete. Based on information gained from the petrographic analysis, the ERDC was also tasked with identifying causes of the distress.

Table 2. Summary of cores received, corresponding CMB Serial No, construction date and testing performed.

Core Sample ID	Floor Placement Number	CMB Serial No.	Testing
1	6	160051-1	Optical microscopy, electron microscopy, elemental mapping, pH indicator measurements, air void analysis
2	6	160051-2	Optical microscopy
3	7	160051-3	Optical microscopy, electron microscopy, elemental mapping, pH indicator measurements, air void analysis
4	7	160051-4	Optical microscopy
5	8	160051-5	Optical microscopy, electron microscopy, elemental mapping, pH indicator measurements, air void analysis

## **3 Experimental Methods**

The following describes the methods used to analyze the five concrete cores from SDU6. As noted in Table 2, all cores were subjected to optical microscopy to identify crack depths and sizes as well as to analyze the microstructure of the concrete. Only cores 1, 3, and 5 were subjected to additional analysis including electron microscopy, elemental mapping, pH indicator measurements, and air void analysis. Cores 1, 3, and 5 were down-selected for these measurements because they were representative of concrete from the three different floor slabs of interest.

### **3.1 Optical Microscopy**

The depth and sizes of cracks along with the microstructure of the concrete was analyzed according to ASTM C856 - *Standard Practice for Petrographic Examination of Hardened Concrete*. Each core was cross sectioned down its long axis prior to polishing to allow for full-depth analysis of cracks through the floor slab as well as the distribution of the microstructure of the concrete from the top to the bottom of the slab. The cross sections were polished using a diamond doped ceramic pad up to 4000 grit (approximately 5  $\mu\text{m}$ ). The polished sample was imaged using a Zeiss Stereo Discovery V20 microscope at magnifications of 5 X to 40 X. Multiple sites were investigated from the surface of the concrete to the bottom of the slab. Additional sites were also investigated if defects were noted or other relevant features in the microstructure such as voids or epoxy infilling of cracks.

### **3.2 Scanning Electron Microscopy and Elemental Mapping**

The same samples prepared for optical microscopy were also used for scanning electron microscopy (SEM). The primary purpose of the SEM imaging was to identify features in the paste microstructure, cracks which were too small to image using optical microscopy, and to better understand epoxy infilling of cracks. SEM imaging was performed using an FEI Nova NanoSEM 630 field emission environmental scanning electron microscopy. Imaging was performed in low-vacuum to minimize charging at an accelerating voltage of 15 kV. Images were taken at magnifications of 100 X to 8,000 X at at least three randomly selected sites on each of the three samples extracted from each floor placement.

In conjunction with SEM imaging, X-ray chemical microanalysis was

performed using a Bruker AXS energy-dispersive x-ray spectrometer (EDS) installed in the SEM. EDS analysis consisted of elemental mapping of Ca, Fe, Al, and Si to aid in identification of phases present in the hydrated cement paste microstructure of the concrete. For EDS analyses, the accelerating voltage was maintained at 15 kV.

### 3.3 pH Indicator Mapping with Optical Microscopy

In order to investigate small changes in pH of the concrete pore solution due to environmental interactions, a Phenolphthalein pH indicator solution was used to stain freshly polished surfaces of the concrete specimens. This indicator exhibits a bright pink colour when exposed to alkaline concrete and remains clear when concrete has a pH below  $\sim 10$ . This measurement was used to identify the cause of discoloration of the paste microstructure adjacent to concrete surfaces and on the faces which may be caused by carbonation, exposure to acidic water (e.g., when the tank was leak tested with mildly acidic water with pH of  $\sim 3.5$ ), or oxidation of the slag rich paste. The use of the pH indicator solution provides information to identify what mechanism is causing the discoloration. Following application of the pH indicator solution, specimens were examined using microscopy techniques described in Section 3.1.

### 3.4 Air Void Analysis

Air void analysis was performed according to the provisions outlined in ASTM C457 – Standard Test Method for Microscopical Determination of Parameters of the Air-Void System in Hardened Concrete. The test method has two procedures; Procedure A, Linear-Traversal Method and Procedure B, Modified Point-Count Method of which was used for this study. Samples were cut and polished cross sections prepared according to ASTM C856 - Standard Practice for Petrographic Examination of Hardened Concrete and analyzed according to Method B of ASTM C457. The minimum length of traverse and minimum number of points for the point count method was determined based on the maximum size of aggregated found in each sample. Calculations for air content were determined on the total number of air voids intersected ( $N$ ), total number of stops ( $S_t$ ), number of stops in air voids ( $S_a$ ), number of stops on paste ( $S_p$ ), and the E-W translation distance between stops ( $I$ ). This information was used to calculate parameters of the air void system including total air content, entrapped air content, entrained air content, and spacing factor.

## 4 Core Sample #1

The typical as-received core from location #1 is shown in Figure 3. A small crack was observed on the top surface of the core (see Figure 4). This crack had been coated by the gravity fed epoxy (see Figure 5). The core was 9.5 cm diameter and 21.6 cm long. One piece of reinforcing steel was included in the core at a depth of approximately 10 cm. The reinforcing steel was located at the edge of the core and was not examined further due to potential degradation in bond during coring. No segregation was observed on the surface of the core and the aggregates and voids appeared to be uniformly distributed. No honeycombs or entrapped air voids were noted.

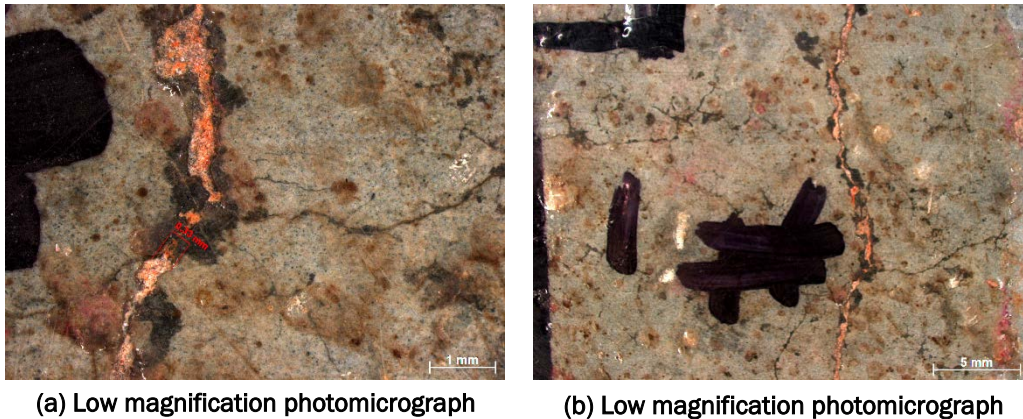
Figure 3. As received concrete Core Sample #1.



Figure 4. Top of Core Sample #1.



Figure 5. Micrographs of crack observed on top of Core Sample #1



#### 4.1 Optical Microscopy

A low magnification montage of images of the sectioned surface of the concrete and the crack observed in Core Sample #1 is shown in Figures 6 and 7. This crack extended to approximately 5 cm in depth into the concrete with a width of approximately 100  $\mu\text{m}$  near the top surface of the crack (see Figure 8). At depths greater than 5 cm, the crack width reduced significantly and appeared to have largely healed itself. Smaller microcracks observed in the paste fraction of the concrete with widths of single to tens of  $\mu\text{m}$  appeared to be self-healed. Examples of these self-healed cracks are shown in Figure 9 and 10. These cracks exhibited white colored mineral deposits likely formed by additional hydration of unhydrated cement grains, precipitation of calcite, or supplementary pozzolanic reactions from unreacted supplementary cementitious materials (e.g., slag, fly ash). Examples of cracks intersecting coarse aggregates were observed (see Figure 7). This suggests that cracking occurred at later ages when concrete had gained sufficient tensile strength to cause cracking of the aggregate rather than debonding around aggregate interfaces and in the paste fraction of the concrete. No vertical displacement was observed between the faces of the crack. The paste appeared as anticipated, with a greenish color in interior portions of the concrete associated with the high slag content of the concrete. Although it was difficult to identify with optical microscopy, epoxy was observed within the crack to depths in excess of 5 cm from the top surface of the concrete (see Figure 11). Overall, the concrete appeared to be of competent quality with no additional defects other than the crack running vertically through the slab. Smaller microcracks in the near surface concrete and

throughout the paste appear to have largely self healed. Discoloration of the concrete was observed to a depth of approximately 1 mm although it was unclear whether this was caused by oxidation of slag in the paste, carbonation of the concrete, or exposure to acidic water.

Figure 6. Montage of optical micrographs of top six inches of concrete from Core Sample #1. Crack in top approximately 5 cm of concrete appears to thin and self heal at greater depths.

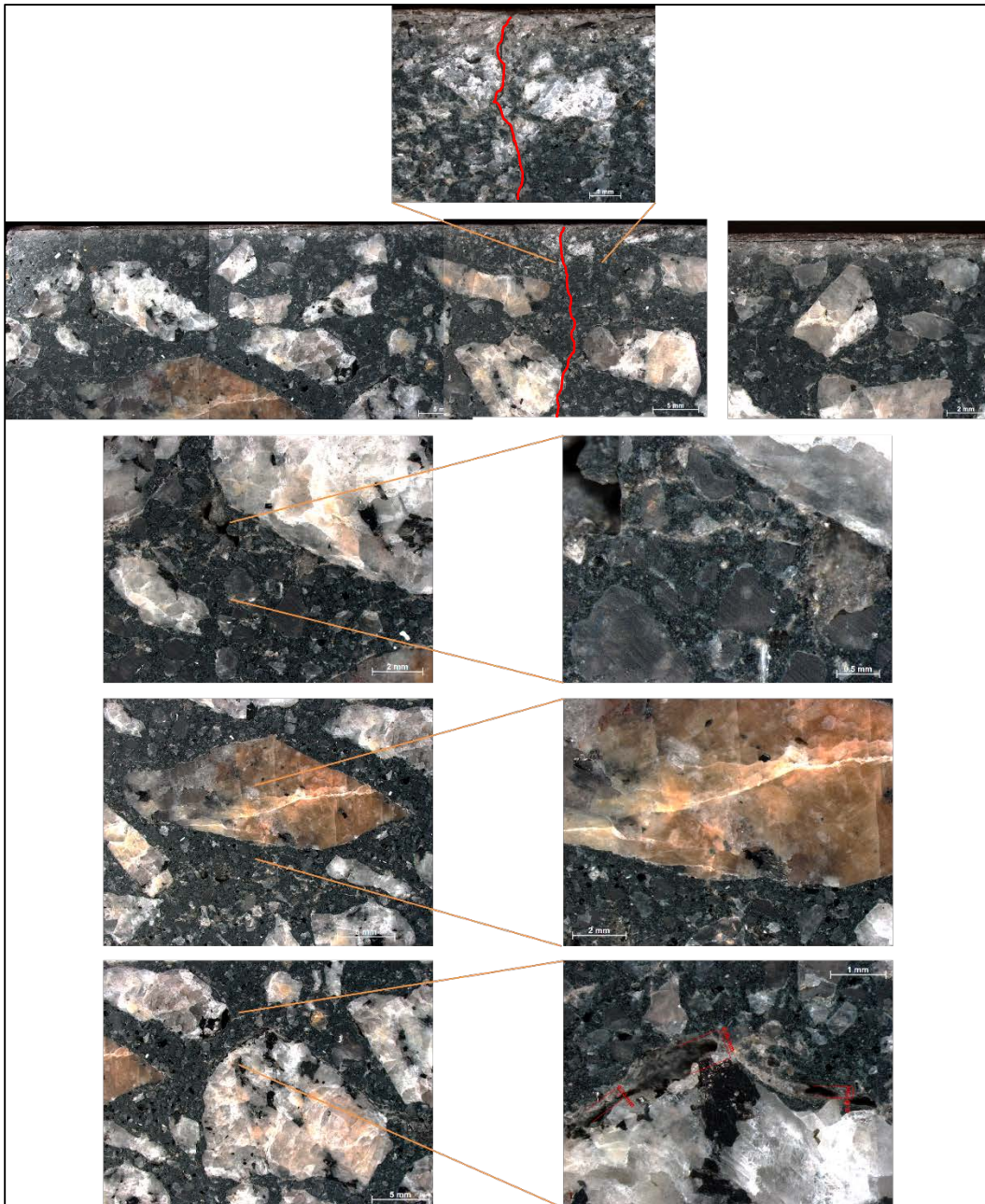


Figure 7. Montage of optical micrographs of bottom 15 cm of concrete from Core Sample #1. Crack observed but faint and appears to be self healed.

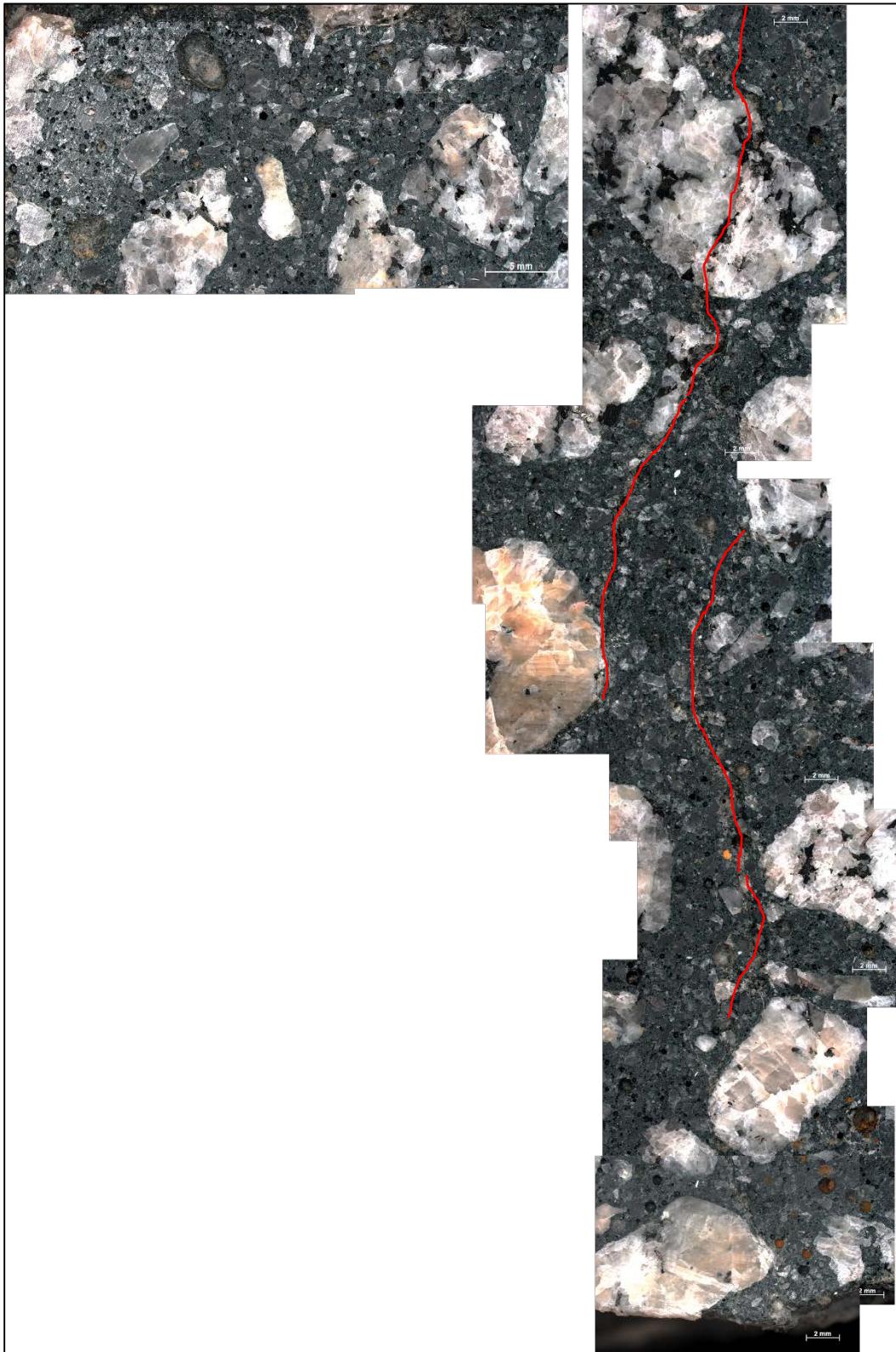


Figure 8. Crack adjacent to top surface of concrete with crack widths of approximately 0.1 mm.

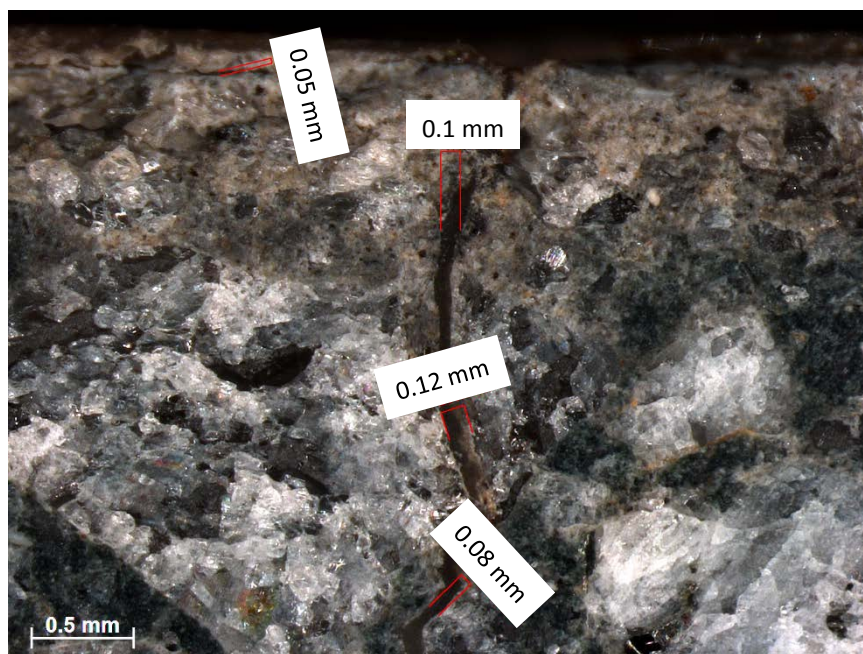


Figure 9. Self healed crack in paste fraction of concrete.

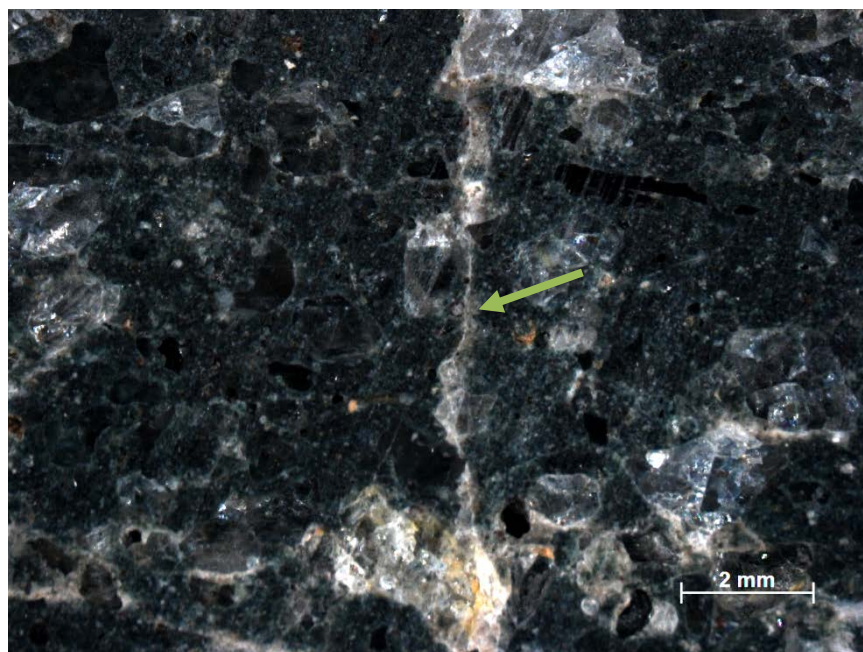


Figure 10. Self healed crack in paste fraction of concrete.

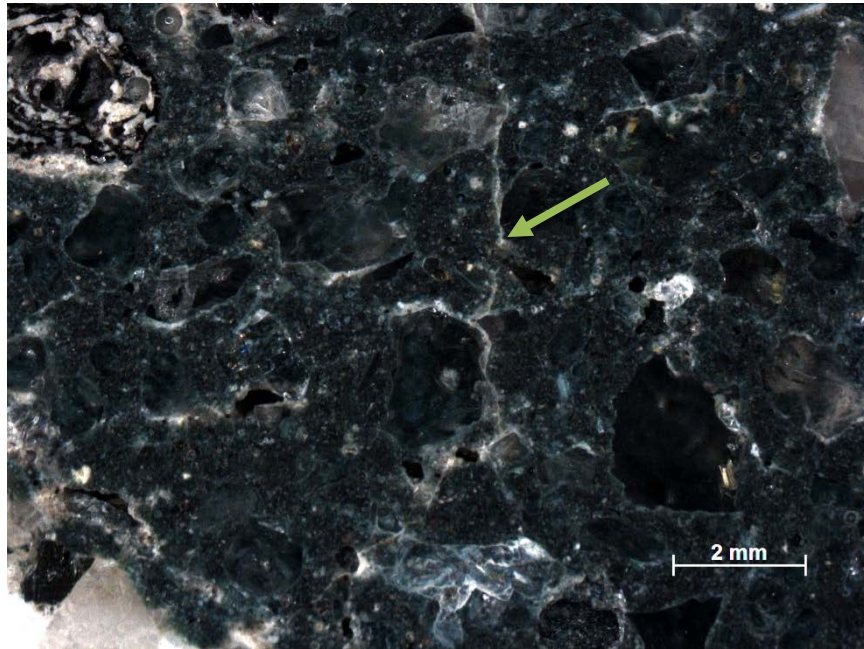


Figure 11. Brown colored epoxy observed to impregnate crack adjacent to concrete surface.



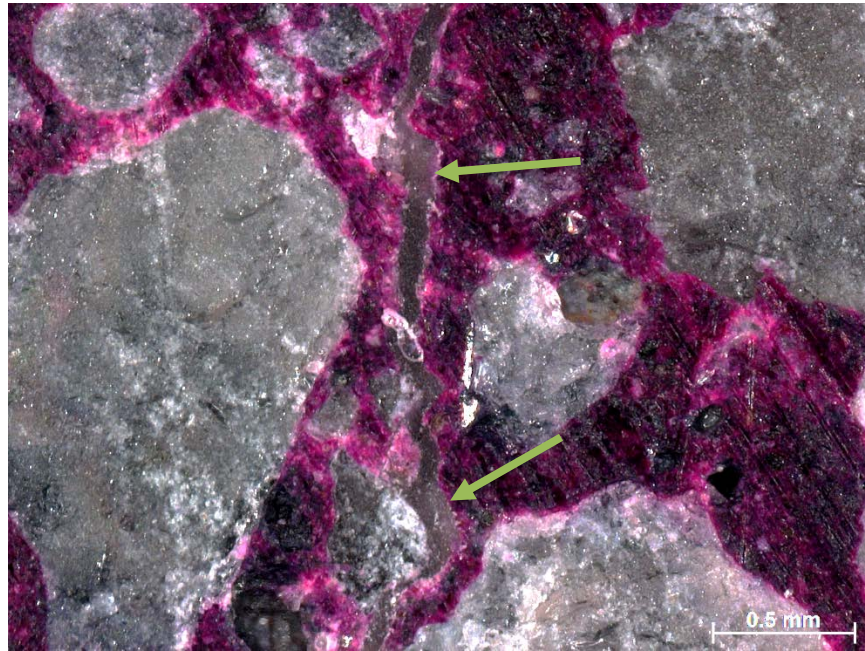
## 4.2 pH Indicator Solution and Microscopy

Figures 12 and 13 show examples of pink staining observed following the application of the pH indicator solution. No staining was observed in the top approximately 1 mm of concrete. Within the concrete, staining was observed adjacent to the crack face and epoxy impregnating the crack. Discoloration of the paste in the near surface of the concrete was associated with some reduction in pH and this is likely due to carbonation and anticipated based on the age of the concrete and its low buffering capacity. Discoloration on the faces of the crack does not appear to be associated with a pH reduction and therefore is likely associated with oxidation of the slag-rich paste rather than carbonation and or acid attack of the concrete.

Figure 12. Staining of paste with pH indicator solution evidencing low pH of near surface concrete but no effect on inner concrete with staining observed adjacent to crack and epoxy in the crack.



Figure 13. Staining of paste indicating high pH adjacent to crack and epoxy within the crack.



### 4.3 Electron Microscopy and Elemental Mapping

A low magnification montage image of the concrete microstructure is shown in Figure 14, with the presence of coarse and fine aggregates as well as paste and pores indicated. Higher magnification imaging of the polished paste microstructure indicated anticipated phases. An example of the microstructure observed at higher magnification is shown in Figure 15. Unreacted fly ash, slag, and cement particles were observed with the fly ash particles being spherical in shape and unreacted cement and slag particles being angular. Smaller silica fume particles were observed as sub-micron sized spheres distributed throughout the paste. The paste appeared to be dense and near full reaction, with minimal porosity. The water-to-cementitious materials ratio appeared to be less than 0.40 based on the minimal porosity observed. At higher magnification, distributed microcracking was observed which is likely due to shrinkage (drying or autogenous) (see Figure 16). Epoxy was observed to have infilled the crack in the near surface concrete. The epoxy infilling appeared to be effecting in a majority of the crack with the exception of areas where the crack intersected a large void. An example of this cracking and the partial infilling with epoxy is shown in Figure 17.

Figure 14. Low magnification montage of concrete microstructure.

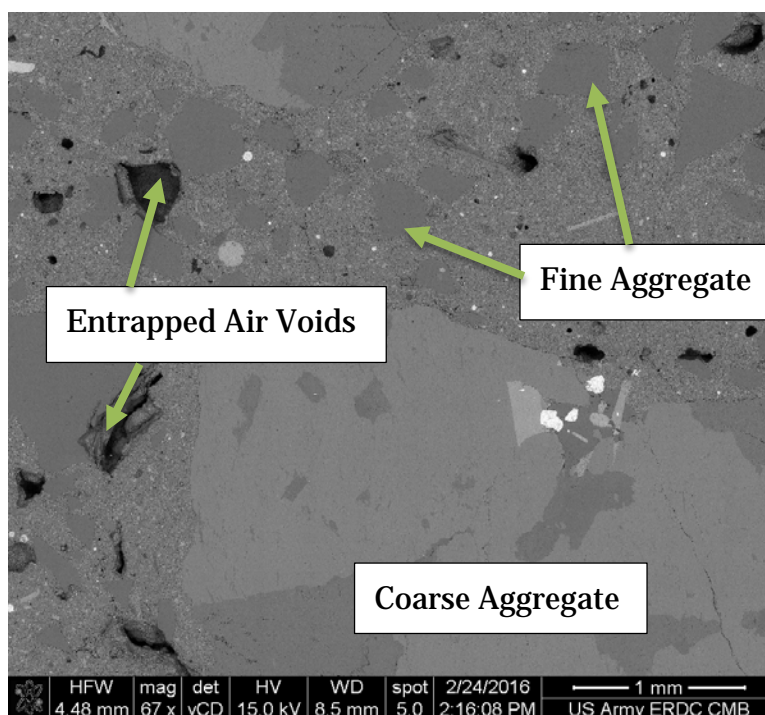


Figure 15. High magnification image of paste microstructure.

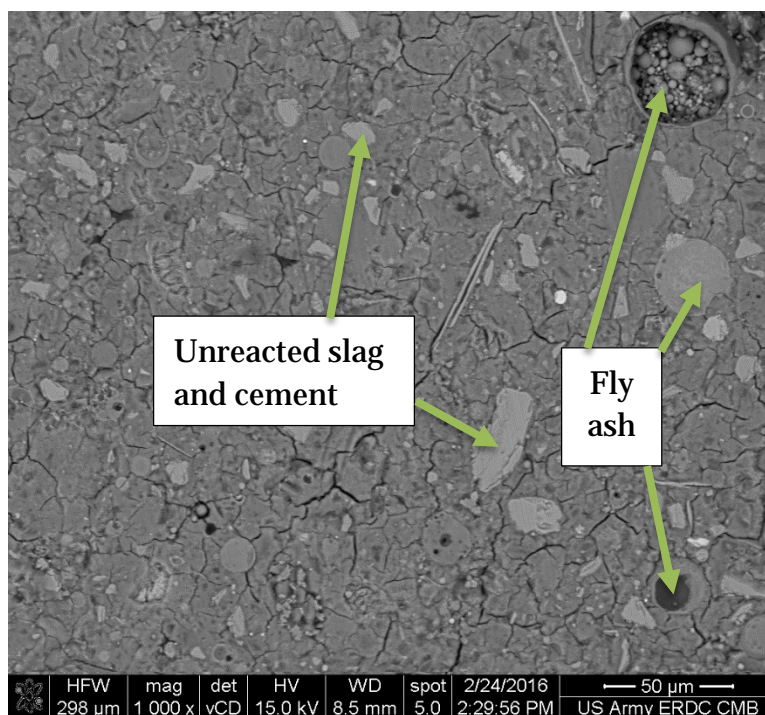


Figure 16. Distributed microcracking observed in paste.

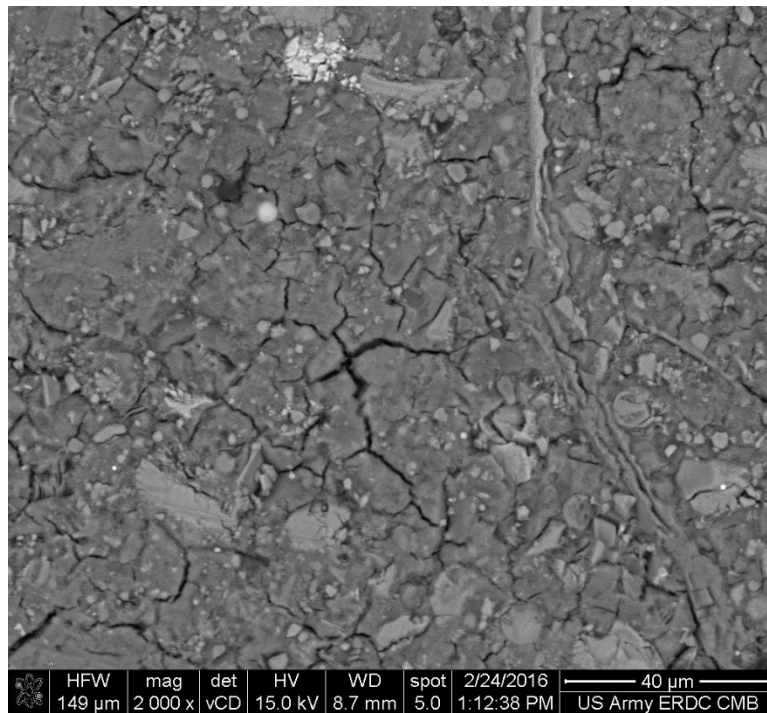
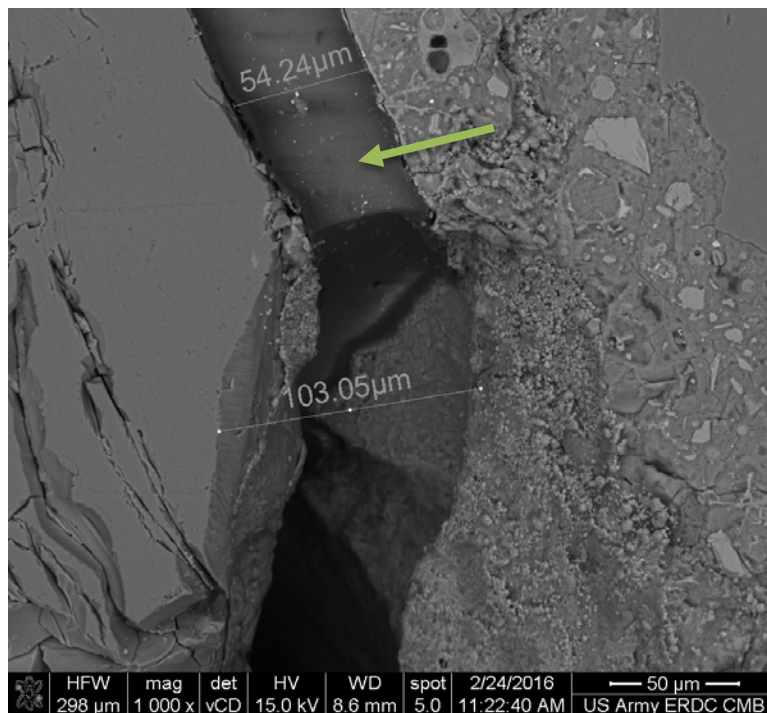
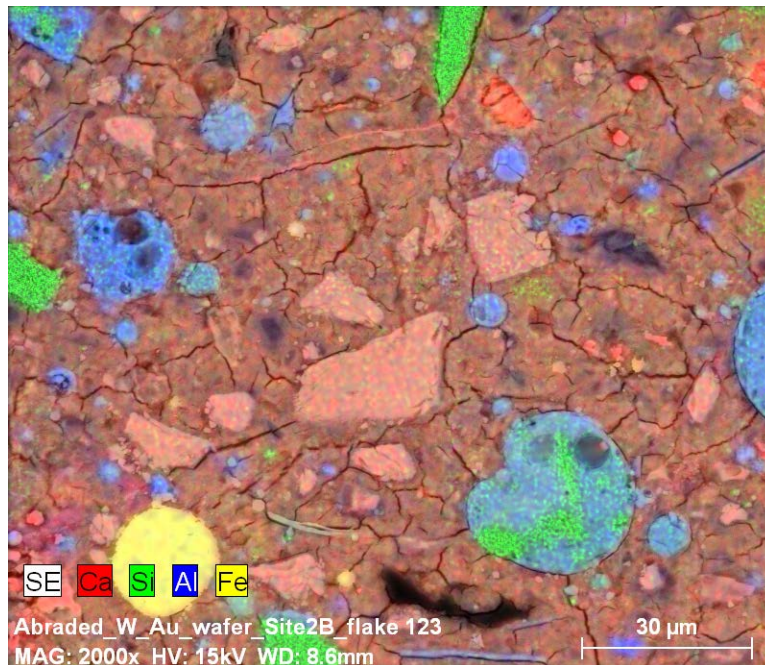


Figure 17. Crack at interface with coarse aggregate with epoxy infilling top portion of crack with 54  $\mu$ m width but with the crack voided in the larger 103  $\mu$ m wide cracked area. Epoxy noted by green arrow.



An elemental map of the paste microstructure typically observed in Core Sample #1 is shown in Figure 18 with colors to note the location of Ca, Si, Al, and Fe rich regions which can be used to identify the location of fly ash, slag, siliceous aggregates, calcium hydroxide, silica fume, and unhydrated cement particles. The anticipated microstructure was observed in the elemental maps. Blue / green spherical particles were unreacted fly ash particles. Larger Si-rich particles are likely contributed by the fine aggregates. Minimal free lime (calcium hydroxide) was observed. Angular particles with red / green color indicative of cement dominated the unreacted phases followed by slag. Overall, the microstructure corresponded to the mixture proportion with a significant proportion of unreacted phases which are anticipated based on the low w/cm and high supplementary cementitious materials content in the concrete used.

Figure 18. Elemental map with Ca, Si, Al, and Fe indicated.



#### 4.4 Air Void Analysis

The entrained and entrapped air contents were 6.2% and 3.9%, respectively, for a total air content of approximately 10%. The spacing factor was 0.38 mm, slightly higher than the 0.2 mm typically considered applicable for freeze/thaw resistance of concrete.

## 5 Core Sample #2

The typical as-received core from location #2 is shown in Figure 19. The core was 7 cm in diameter and 30.5 long. No cracks were observed by visual inspection of Core Sample #2 upon examination of the top surface and sides of the core (see Figure 20). No segregation was observed on the surface of the core and the aggregates and voids appeared to be uniformly distributed. No large honeycombs or entrapped air voids were noted.

Figure 19. As received core sample #2.



Figure 20. Top surface of core sample #2.



## 5.1 Optical Microscopy

No large cracks with sizes greater than 10  $\mu\text{m}$  were observed in Core Sample #2. As a result, no low magnification montages to map cracks through the depth of the concrete were assembled. Smaller microcracks observed in the paste fraction of the concrete with widths of single  $\mu\text{m}$  appeared to be self-healed. Examples of these self healed cracks are shown in Figure 21. These cracks exhibited white colored mineral deposits likely formed by additional hydration of unhydrated cement grains, precipitation of calcite, or supplementary pozzolanic reactions from unreacted supplementary cementitious materials (e.g., slag, fly ash). No vertical displacement was observed between the faces of the crack. The paste appeared as anticipated and similar to that observed in Core Sample #1, with a greenish color in interior portions of the concrete associated with the high slag content of the concrete. Regions of what appeared to be poorly mixed or reacted paste were observed (see Figure 22) although these did not appear to be causing any additional distress. Overall, the concrete appeared to be of competent quality with no additional defects other than the crack running vertically through the slab. Smaller microcracks appear to have largely self healed. Discoloration of the concrete was observed to a depth of approximately 1 mm.

Figure 21. Microcracking in near-surface concrete with white colored infilling from mineral self healing of cracks.



Figure 22. Typical paste microstructure. Spherical air voids observed throughout the paste. Sparse regions of gray / taupe colored poorly reacted paste noted by green arrow.



## 6 Core Sample #3

The typical as-received core from location #3 is shown in Figure 23. A small crack was observed on the top surface of the core (see Figure 24). This crack had been coated by the gravity fed epoxy. The core was 7 cm in diameter and 30.5 cm long. No segregation was observed on the surface of the core and the aggregates and voids appeared to be uniformly distributed. No large honeycombs or entrapped air voids were noted.

Figure 23. As received Core Sample #3.

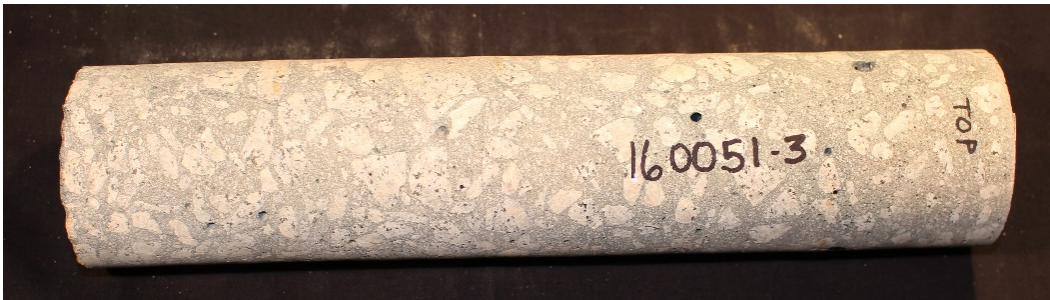


Figure 24. Top surface of Core Sample #3 with crack location noted.



## 6.1 Optical Microscopy

A low magnification montage of images of the sectioned surface of the concrete and the crack observed in Core Sample #3 is shown in Figures 25 and 26. Crack widths in the first two inches of concrete ranged from 0.1 to 0.2 mm in width (see Figure 27). Smaller microcracks observed in the paste appeared to be self healed with mineral infilling of cracks (see Figure 28). Cracks were noted to sparsely intersect with coarse aggregates (see Figure 26). This suggests that cracking occurred at later ages when concrete had gained sufficient tensile strength to cause cracking of the aggregate rather than debonding around aggregate interfaces and in the paste fraction of the concrete. Higher magnification imaging of the primary crack observed in the core indicated successful infilling of the crack with full infilling of the crack itself and coloring of the faces of the crack likely associated with epoxy impregnation of the paste. An example of this successful infilling is shown in Figure 29. No vertical displacement was observed between the faces of the crack. The paste appeared as anticipated, with a greenish color in interior portions of the concrete associated with the high slag content of the concrete. Overall, the concrete appeared to be of competent quality with no additional defects other than the crack running vertically through the slab.

Figure 25. Low magnification montage of the crack observed in the top 15 cm of concrete from Core Sample #3. The crack extended the full length of the core with discoloration observed at the top surface and inner faces of the crack. Infilling of epoxy observed in the crack.

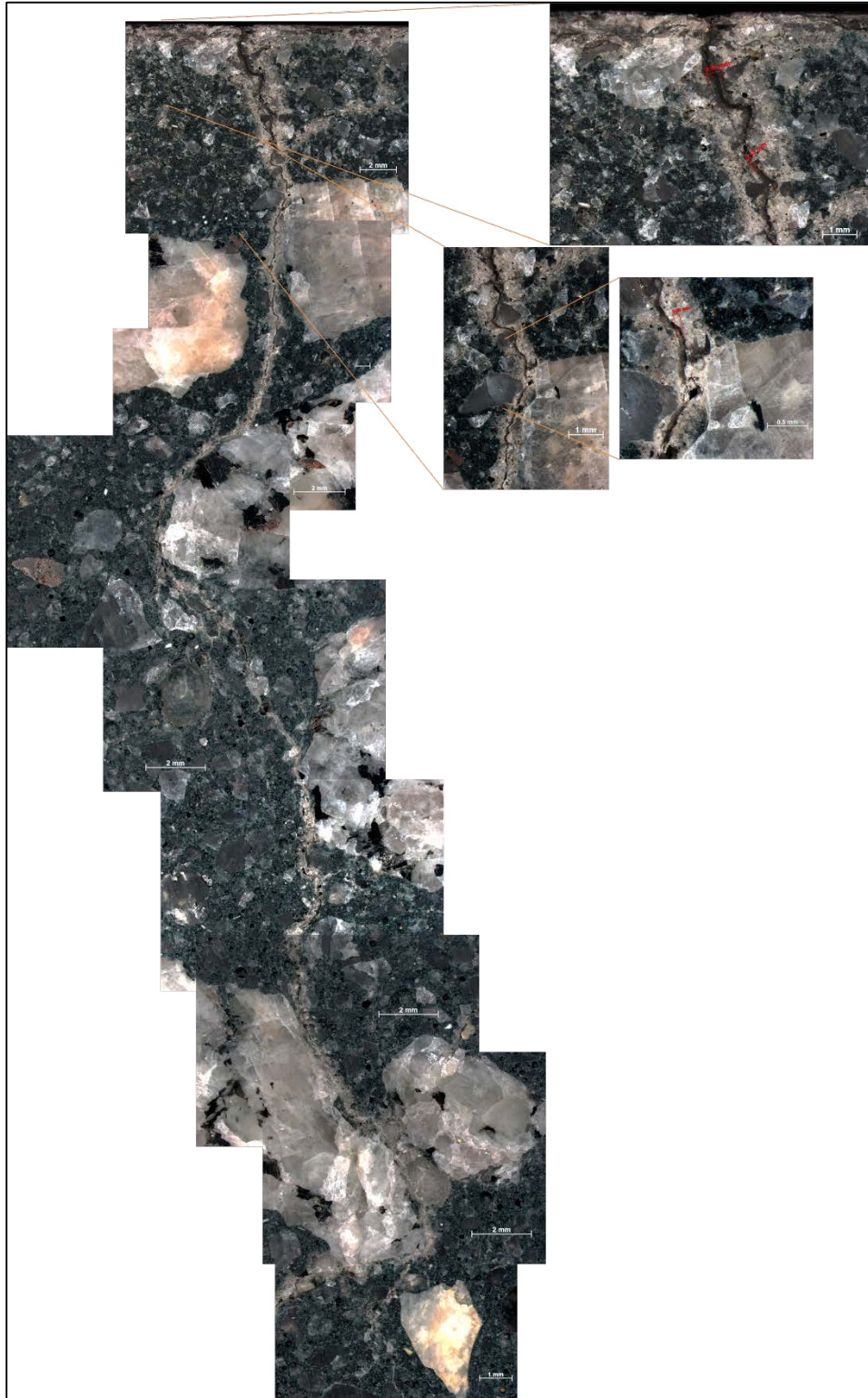


Figure 26. Low magnification montage of crack through the bottom portion of Core Sample #3. Crack intersecting coarse aggregate noted with green arrow.



Figure 27. Low magnification image of crack adjacent to surface. Discoloration of concrete observed in top approximately 2 mm of concrete as well as down the length of the crack. Crack widths range from 0.1 to 0.2 mm.

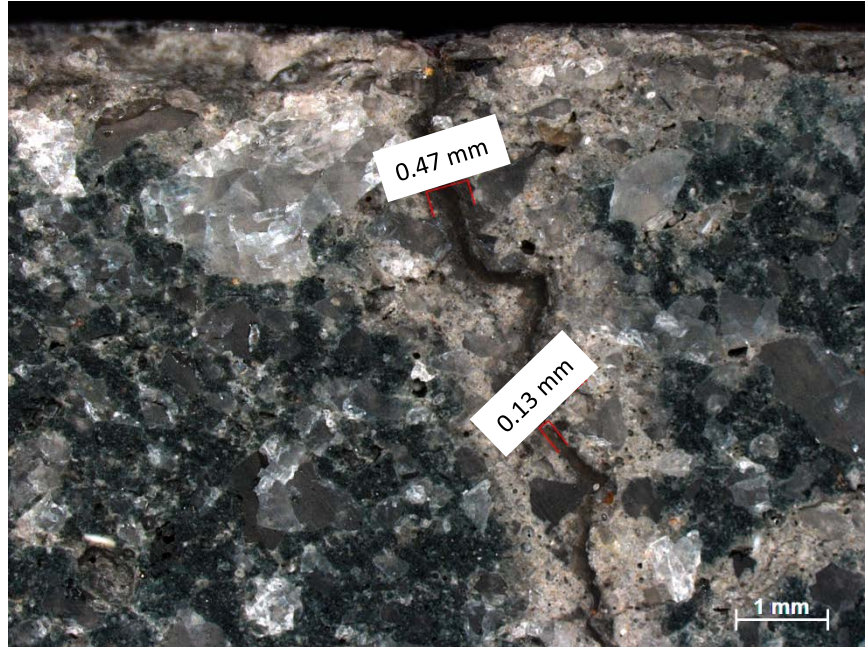


Figure 28. Microcracks in paste fraction of concrete with mineral infilling of crack and self healing.

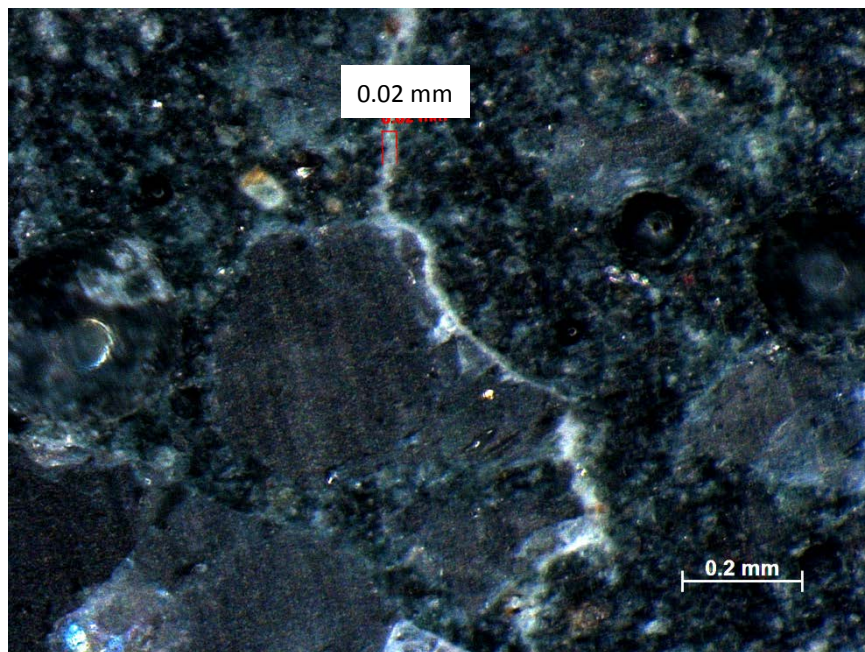
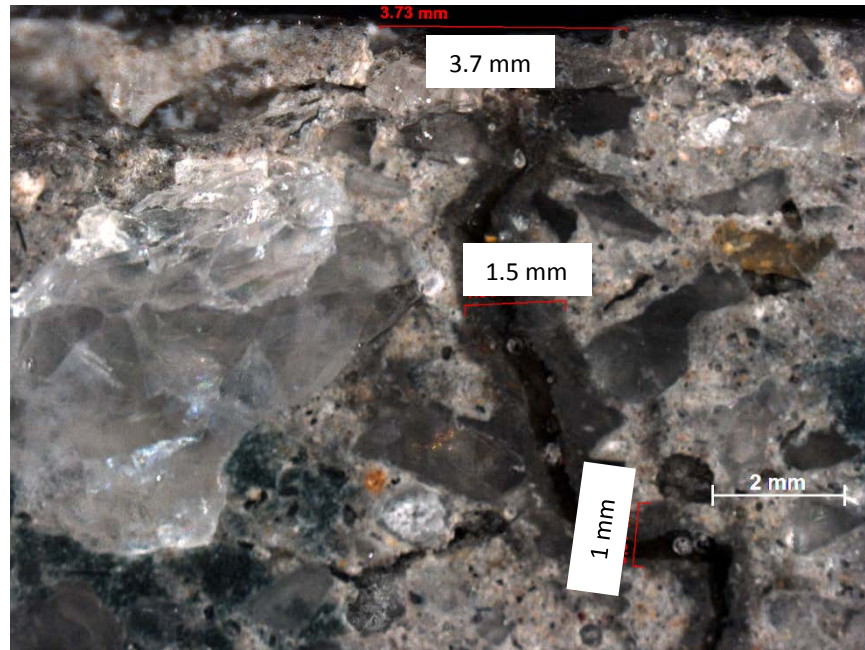


Figure 29. High magnification image of epoxy infilling of crack. Epoxy appears to successfully infill the crack to multiple inches in depth. Discoloration of the faces of the crack was also observed resulting from impregnation of the adjacent paste with epoxy. Discoloration of the paste was also observed at the concrete surface and down the length of the crack.



## 6.2 pH Indicator Solution and Microscopy

Figures 30 and 31 show examples of pink staining observed following the application of the pH indicator solution. No staining was observed in the top approximately 1.5-2 mm of concrete. Within the concrete, staining was observed adjacent to the crack face and epoxy impregnating the crack. Discoloration of the paste in the near surface of the concrete was associated with some reduction in pH and this is likely due to carbonation and anticipated based on the age of the concrete and its low buffering capacity. Discoloration on the faces of the crack does not appear to be associated with a pH reduction and therefore is likely associated with oxidation of the slag-rich paste rather than carbonation and or acid attack of the concrete.

Figure 30. Photomicrograph of concrete following application of pH indicator solution. No staining observed in near surface concrete. Minor staining observed on faces of crack. Strong staining observed in paste fraction.

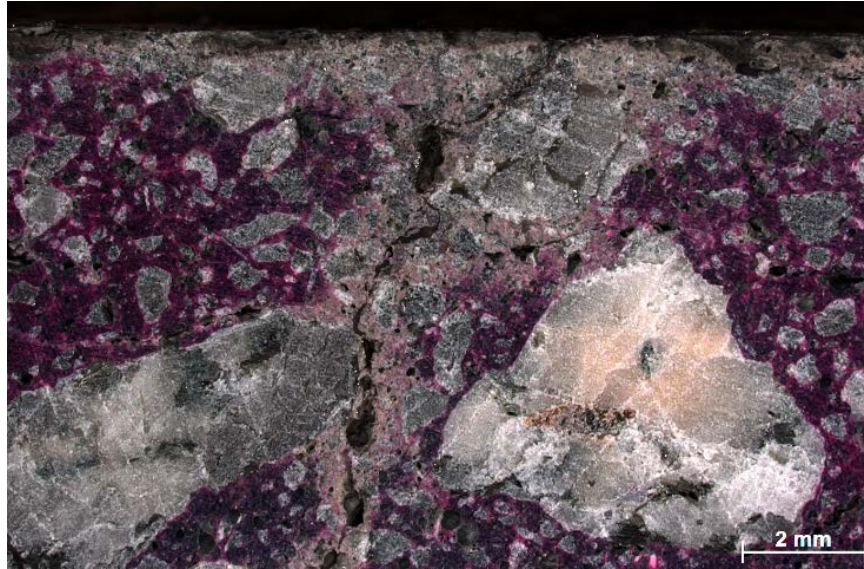
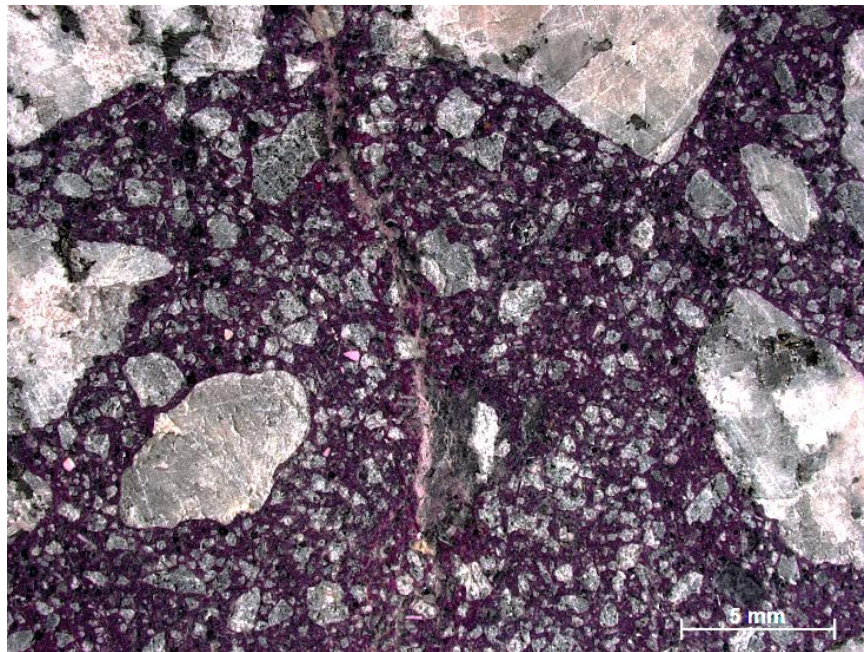


Figure 31. Strong staining of concrete with pH indicator solution completely to faces of crack, indicating that discoloration at face of crack is not associated with a reduction in pH.



### 6.3 Electron Microscopy and Elemental Mapping

Low magnification montage images of the concrete microstructure including the crack adjacent to the surface and at a depth of approximately 7.5 cm are shown in Figures 32 and 33, respectively. Epoxy infilling within the crack in Core Sample #3 was very successful, with full infilling of the crack, no voids observed, and strong adherence to the faces of the crack, likely imparting water tightness to this crack. Higher magnification imaging of the polished paste microstructure indicated anticipated phases similar to those observed in Core Sample #1 when examined using SEM. An example of the microstructure observed at higher magnification is shown in Figure 34. Unreacted fly ash, slag, and cement particles were observed with the fly ash particles being spherical in shape and unreacted cement and slag particles being angular. Smaller silica fume particles were observed as sub-micron sized spheres distributed throughout the paste. The paste appeared to be dense and near full reaction, with minimal porosity. The water-to-cementitious materials ratio appeared to be less than 0.40 based on the minimal porosity observed. At higher magnification, distributed microcracking was observed which is likely due to shrinkage (drying or autogenous).

An elemental map of the paste microstructure typically observed in Core Sample #3 is shown in Figure 35 with colors to note the location of Ca, Si, Al, and Fe rich regions which can be used to identify the location of fly ash, slag, siliceous aggregates, calcium hydroxide, silica fume, and unhydrated cement particles. The anticipated microstructure was observed in the elemental maps. Blue / green spherical particles were unreacted fly ash particles. Larger Si-rich particles are likely contributed by the fine aggregates. Minimal free lime (calcium hydroxide) was observed. Angular particles with red / green color indicative of cement dominated the unreacted phases followed by slag. Overall, the microstructure corresponded to the mixture proportion with a significant proportion of unreacted phases which are anticipated based on the low w/cm and high supplementary cementitious materials content in the concrete used.

Figure 32. Vertical crack through Core Sample #3 with infilling of the crack with epoxy.

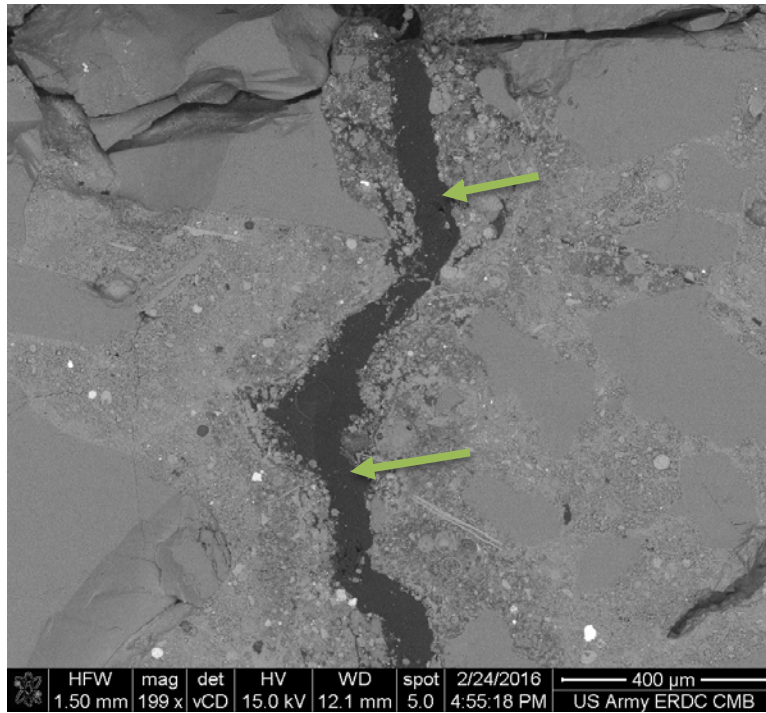


Figure 33. Vertical crack through Core Sample #3 at depth of approximately 7.5 cm with full infilling of crack with epoxy.

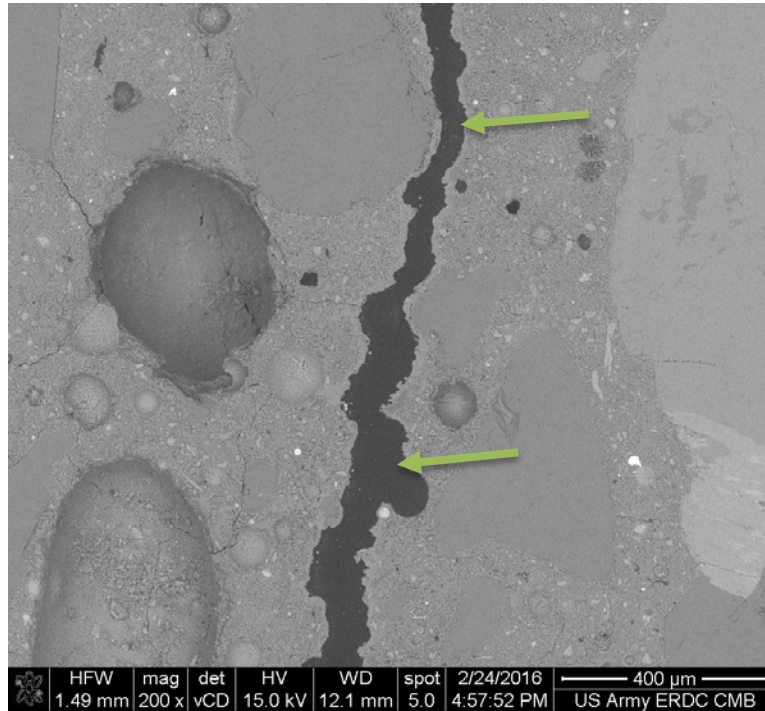


Figure 34. Typical paste microstructure with microcracking observed. Larger spherical particles associated with unreacted fly ash. Larger angular particles

associated with untreated cement and slag. Very dense hydrated cement paste microstructure with minimal porosity.

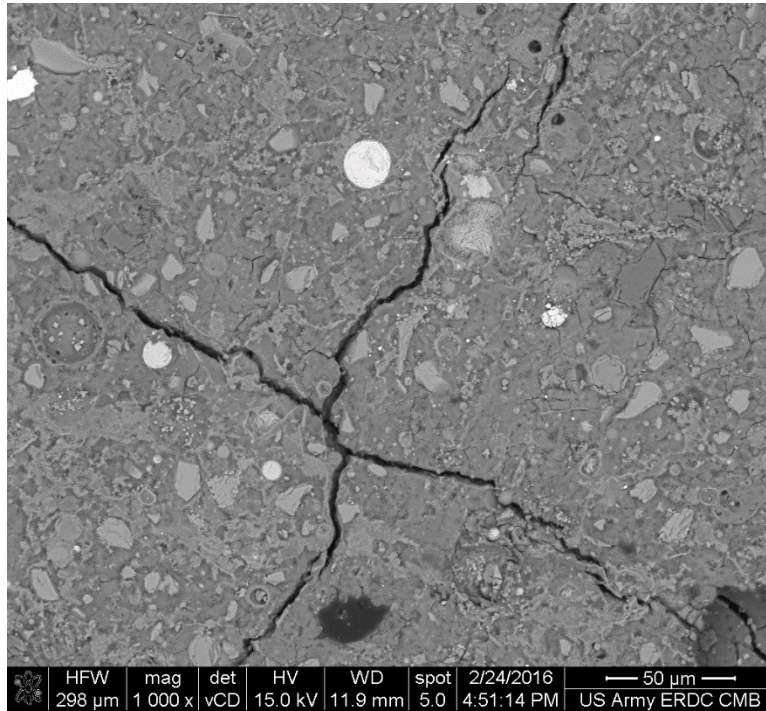
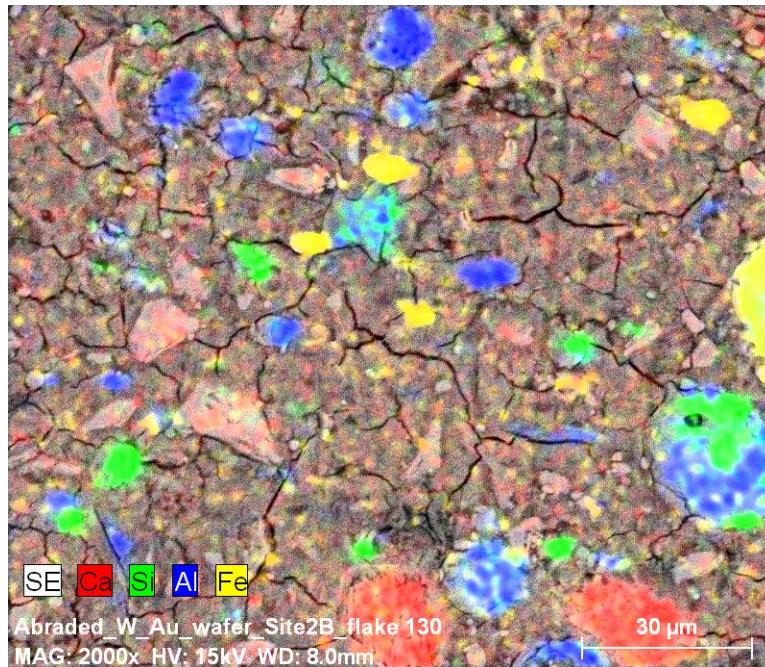


Figure 35. Elemental map with Ca, Si, Al, and Fe noted based on colors to aid in identification of phases in hydrated cement paste microstructure.



#### 6.4 Air Void Analysis

The entrained and entrapped air contents were 9.1% and 1.3%, respectively, for a total air content of approximately 10.4%. The spacing factor was 0.38 mm, slightly higher than the 0.2 mm typically considered applicable for freeze/thaw resistance of concrete.

## 7 Core Sample #4

The typical as-received core from location #4 is shown in Figure 36. A small crack was observed on the top surface of the core (see Figure 37). This crack had been coated by the gravity fed epoxy. The core was 7 cm in diameter and 30.5 cm long. No segregation was observed on the surface of the core and the aggregates and voids appeared to be uniformly distributed. No large honeycombs or entrapped air voids were noted.

Figure 36. As received concrete core sample #4.



Figure 37. Top surface of core sample #4.



## 7.1 Optical Microscopy

A low magnification montage of images of the sectioned surface of the concrete and the crack observed in Core Sample #4 is shown in Figures 38 and 39. Crack widths ranged from 0.2 to 0.5 mm in width (see Figure 40). Cracks were noted to sparsely intersect with coarse aggregates (see Figure 41). This suggests that cracking occurred at later ages when concrete had gained sufficient tensile strength to cause cracking of the aggregate rather than debonding around aggregate interfaces and in the paste fraction of the concrete. No vertical displacement was observed between the faces of the crack. The paste appeared as anticipated, with a greenish color in interior portions of the concrete associated with the high slag content of the concrete. Overall, the concrete appeared to be of competent quality with no additional defects other than the crack running vertically through the slab.

Figure 38. Low magnification montage of upper portion of Core Sample #4 through-depth cracking.



Figure 39. Low magnification montage of cracking in bottom portion of Core Sample #4. Crack extends through full depth of core and through coarse aggregates as noted by green arrows.

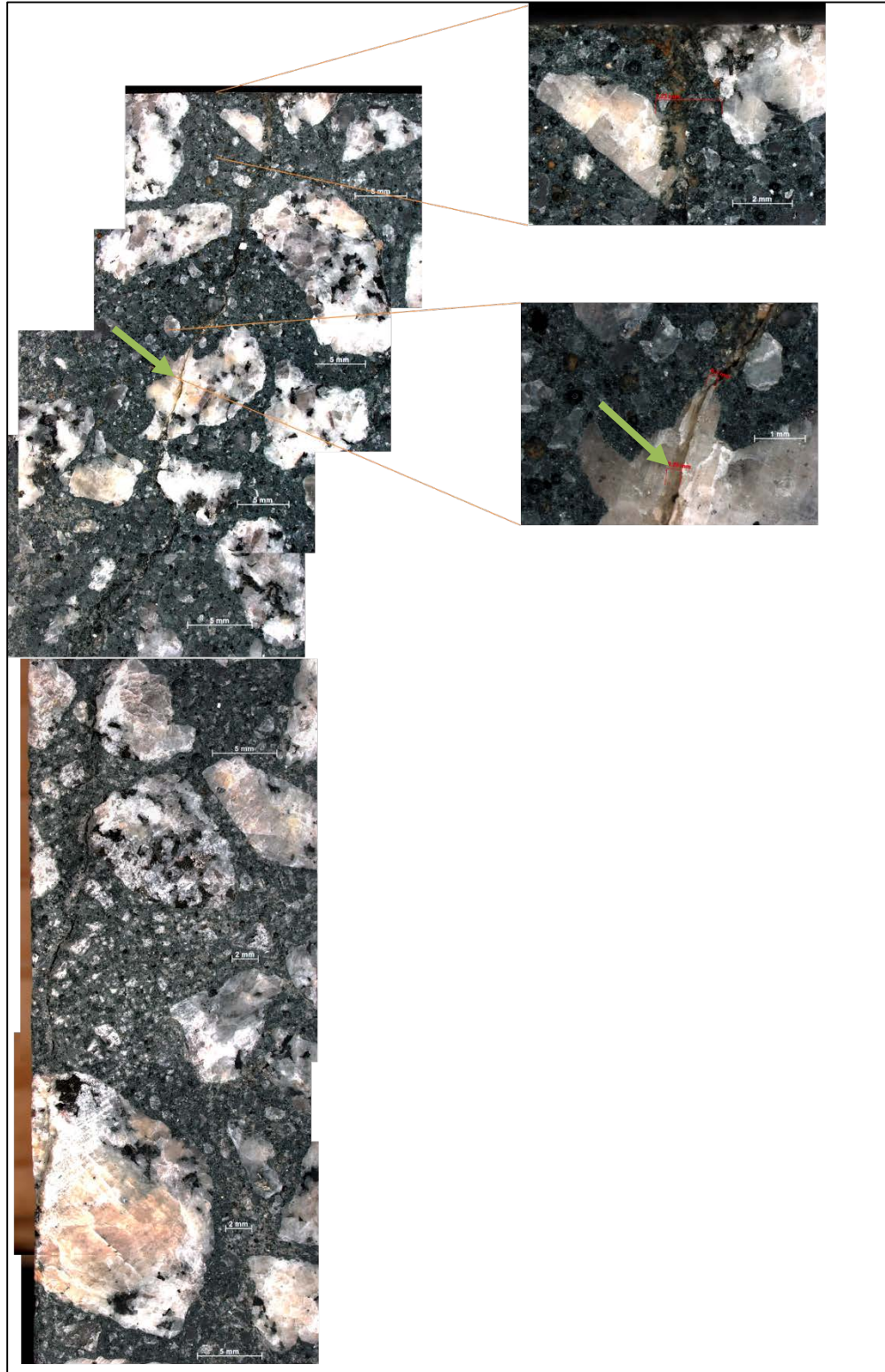


Figure 40. Measurements of crack at concrete surface.

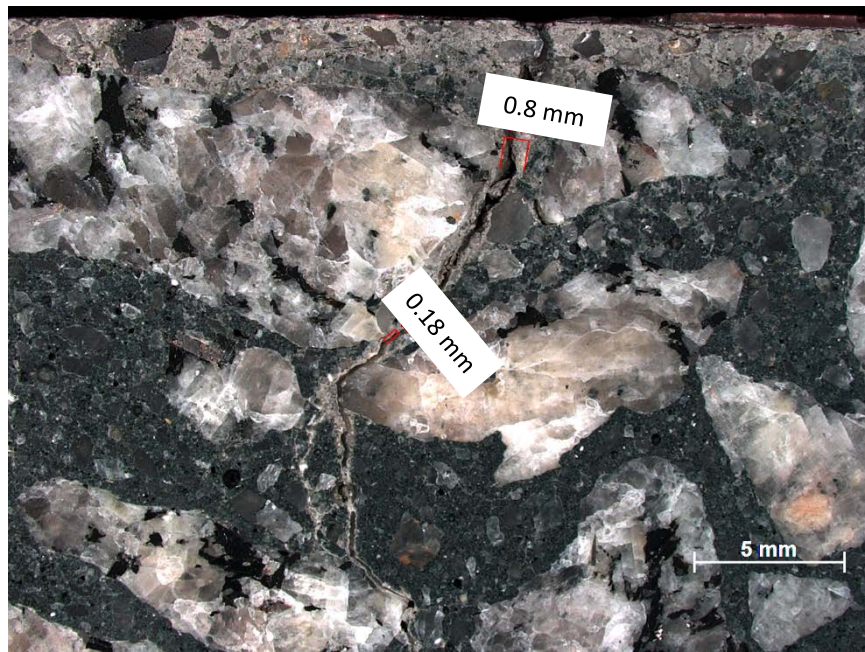


Figure 41. Crack observed through coarse aggregate noted with green arrow.



## 8 Core Sample #5

The typical as-received core from location #5 is shown in Figure 42. A large crack was observed on the top surface of the core (see Figure 43). This crack had been coated by the gravity fed epoxy. The core was 7 cm in diameter and 30.5 cm long. No segregation was observed on the surface of the core and the aggregates and voids appeared to be uniformly distributed. No large honeycombs or entrapped air voids were noted.

Figure 42. As received core sample #5.



Figure 43. Top surface of core sample #5 with crack noted with green arrows.



## 8.1 Optical Microscopy

A low magnification montage of images of the sectioned surface of the concrete and the crack observed in Core Sample #5 is shown in Figures 44 and 45. Core #5 was removed from floor placement 8 which had a high degree of restraint and severe cracking. The crack in Core Sample #5 ran the full depth of the slab, with crack with ranging from 0.5 to 1 mm in the near surface concrete to 0.2 to 0.5 mm in inner portions of the concrete. At higher magnification, cracks were observed to be 0.4 to over 1 mm in width (see Figures 46 and 47). Although epoxy was observed on the top surface of the core, the crack appeared to be void of epoxy. The crack also was observed to intersect 10 coarse aggregates through the depth of the slab. This suggests that cracking occurred at later ages when concrete had gained sufficient tensile strength to cause cracking of the aggregate rather than debonding around aggregate interfaces and in the paste fraction of the concrete. Examples of this cracking are shown in Figures 47 and 48. No vertical displacement was observed between the faces of the crack. The paste appeared as anticipated, with a greenish color in interior portions of the concrete associated with the high slag content of the concrete. Overall, the concrete appeared to be of competent quality with no additional defects other than the crack running vertically through the slab.

Figure 44. Low magnification montage of through depth crack in top portion of Core Sample #5. Crack of 0.5 to 1 mm in width extending to a depth of 7-10 cm with the crack thinning to 0.2-0.5 mm in width at greater depths.

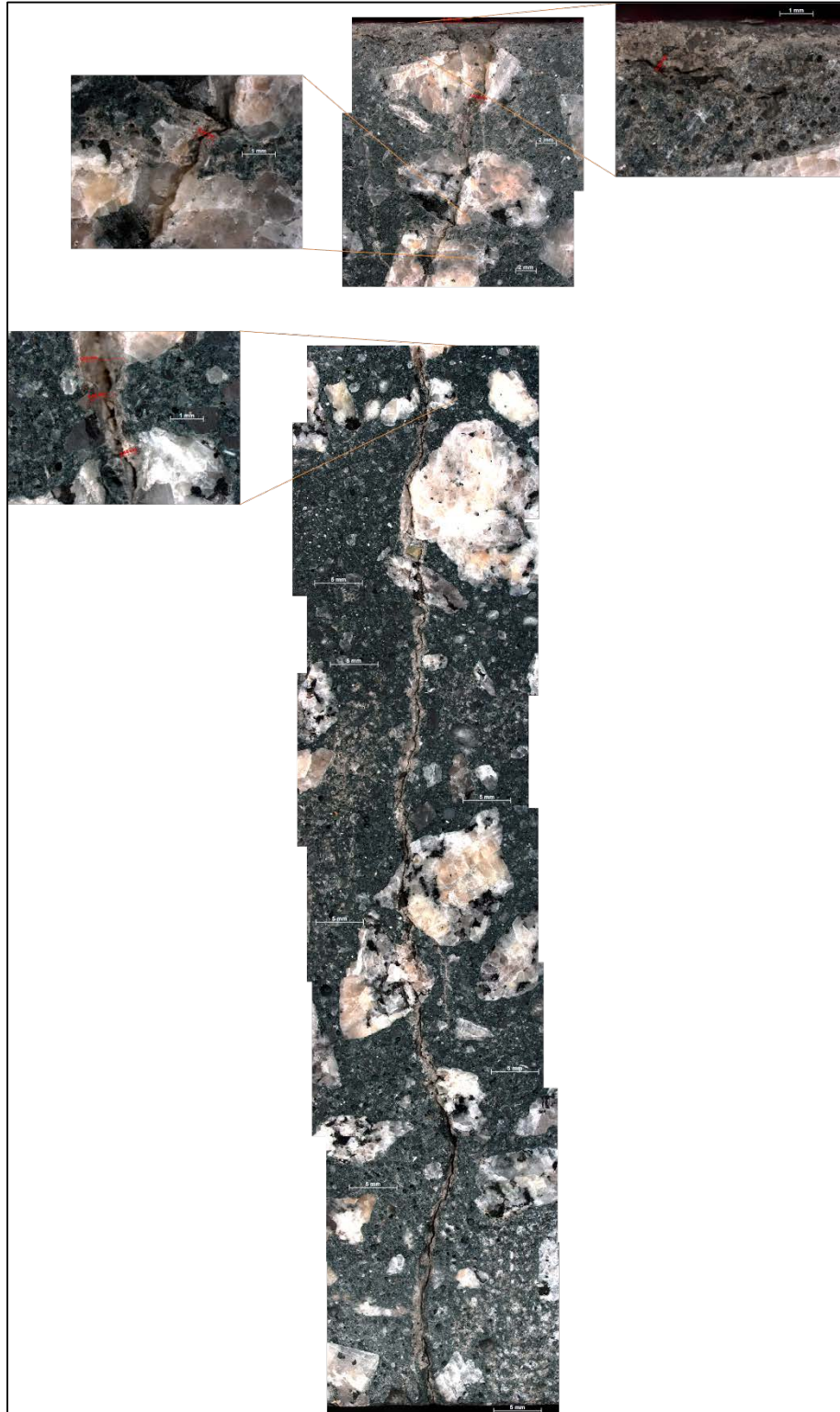


Figure 45. Low magnification montage of crack through the bottom portion of Core Sample #5. Multiple instances of the crack intersecting coarse aggregates.



Figure 46. Imaging of crack near concrete surface with measurements of crack with noted on image.

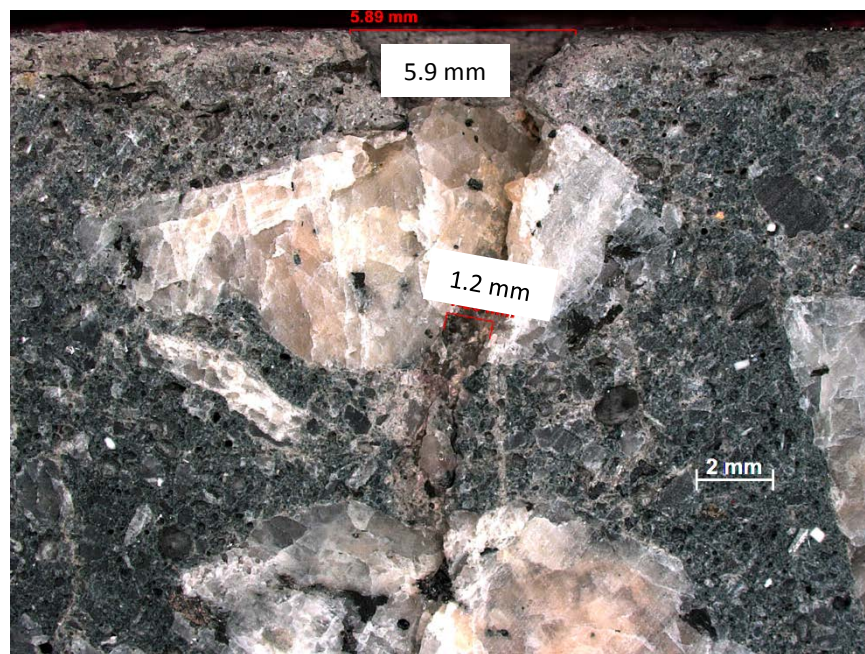


Figure 47. Crack width measurements in bottom portion of core and location of crack intersecting coarse aggregate.

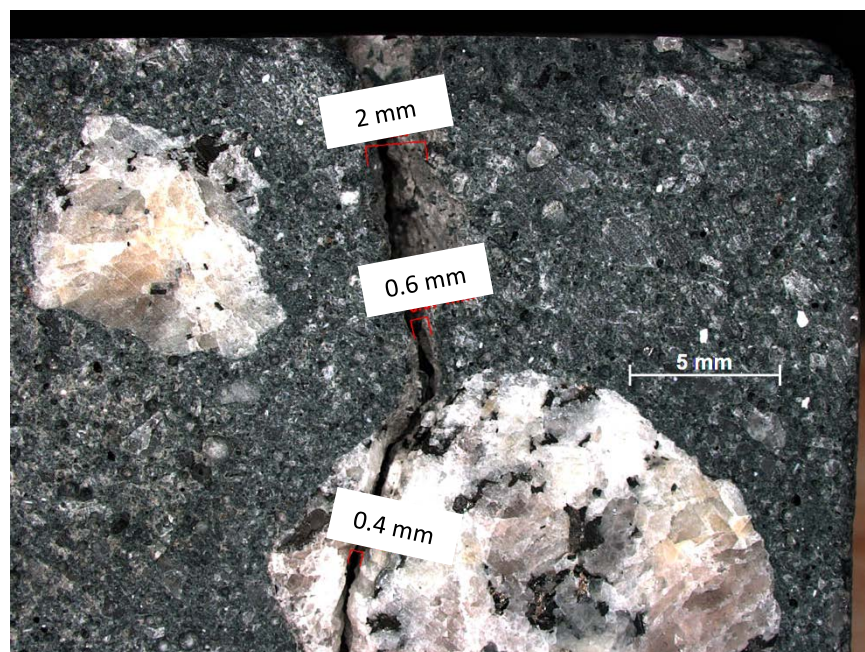


Figure 48. Crack intersecting coarse aggregate.



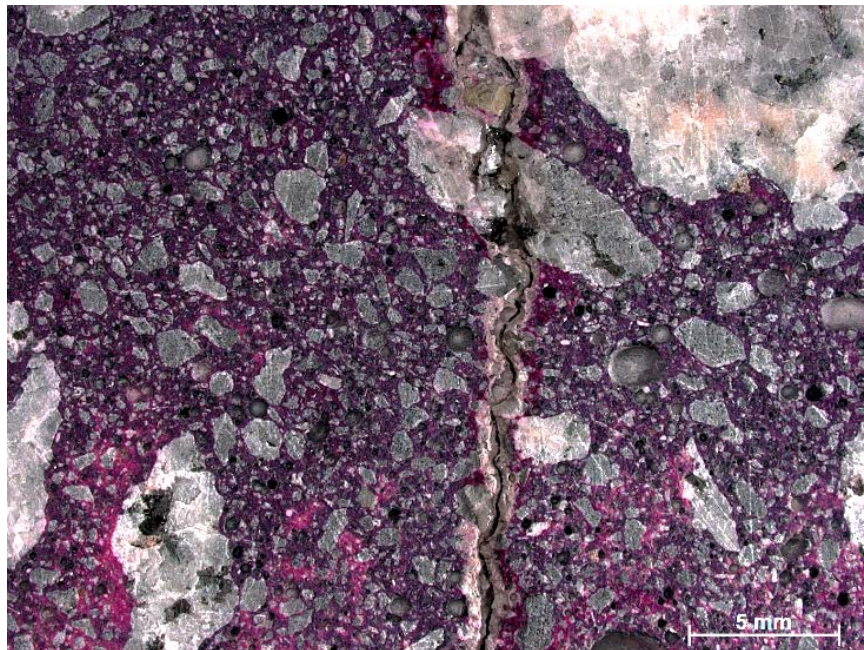
## 8.2 pH Indicator Solution and Microscopy

Figures 49 and 50 show examples of pink staining observed following the application of the pH indicator solution. No staining was observed in the top approximately 1.5-2 mm of concrete. Within the concrete, staining was observed adjacent to the crack face. Discoloration of the paste in the near surface of the concrete was associated with some reduction in pH and this is likely due to carbonation and anticipated based on the age of the concrete and its low buffering capacity. Discoloration on the faces of the crack does not appear to be associated with a pH reduction and therefore is likely associated with oxidation of the slag-rich paste rather than carbonation and or acid attack of the concrete.

Figure 49. Micrograph of result of pH staining test showing no staining at near surface of concrete.



Figure 50. Result of pH indicator solution staining showing strong staining of paste and minor staining of discolored region adjacent to crack face.



### 8.3 Electron Microscopy and Elemental Mapping

A low magnification montage image of the concrete microstructure including the crack adjacent to the surface is shown in Figure 51. No epoxy was observed to infill the crack in Core Sample #5 even after in depth analysis of the full length of the crack. No epoxy was observed on the walls of the crack. Higher magnification imaging of the polished paste microstructure indicated anticipated phases similar to those observed in Core Sample #1 when examined using SEM. An example of the microstructure observed at higher magnification is shown in Figure 52. Unreacted fly ash, slag, and cement particles were observed with the fly ash particles being spherical in shape and unreacted cement and slag particles being angular. Smaller silica fume particles were observed as sub-micron sized spheres distributed throughout the paste. The paste appeared to be dense and near full reaction, with minimal porosity. The water-to-cementitious materials ratio appeared to be less than 0.40 based on the minimal porosity observed. At higher magnification, distributed microcracking was observed which is likely due to shrinkage (drying or autogenous).

An elemental map of the paste microstructure typically observed in Core Sample #5 is shown in Figure 53 with colors to note the location of Ca, Si, Al, and Fe rich regions which can be used to identify the location of fly ash, slag, siliceous aggregates, calcium hydroxide, silica fume, and unhydrated cement particles. The anticipated microstructure was observed in the elemental maps. Blue / green spherical particles were unreacted fly ash particles. Larger Si-rich particles are likely contributed by the fine aggregates. Minimal free lime (calcium hydroxide) was observed. Angular particles with red / green color indicative of cement dominated the unreacted phases followed by slag. Overall, the microstructure corresponded to the mixture proportion with a significant proportion of unreacted phases which are anticipated based on the low w/cm and high supplementary cementitious materials content in the concrete used.

Figure 51. Low magnification montage of crack through coarse aggregate near the concrete surface.

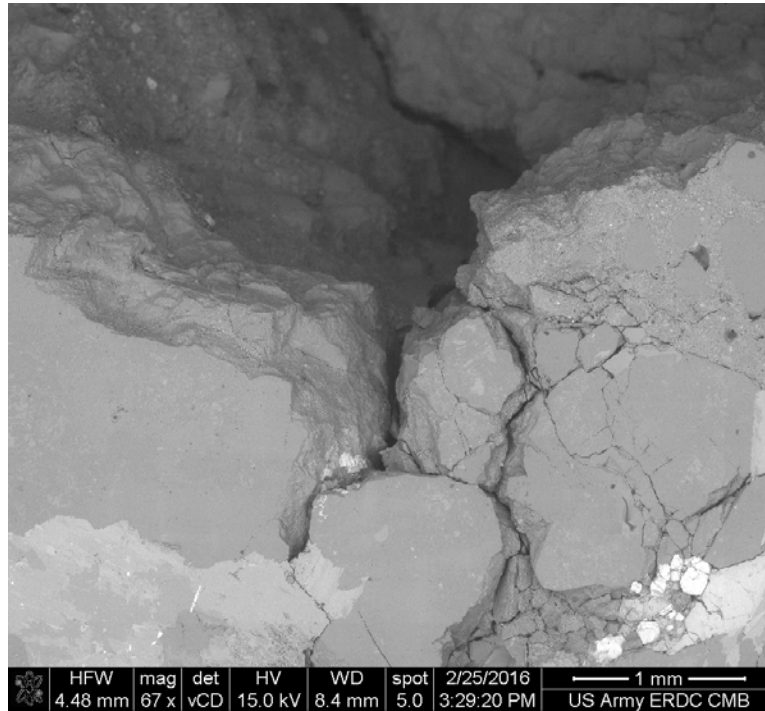


Figure 52. High magnification image of paste microstructure. Spherical particles associated with fly ash. Angular particles associated with unreacted slag and cement particles.

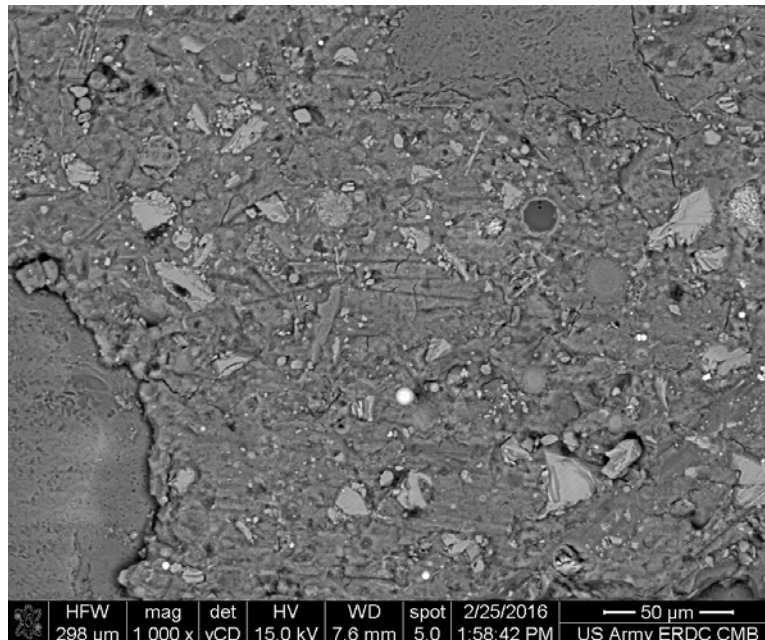
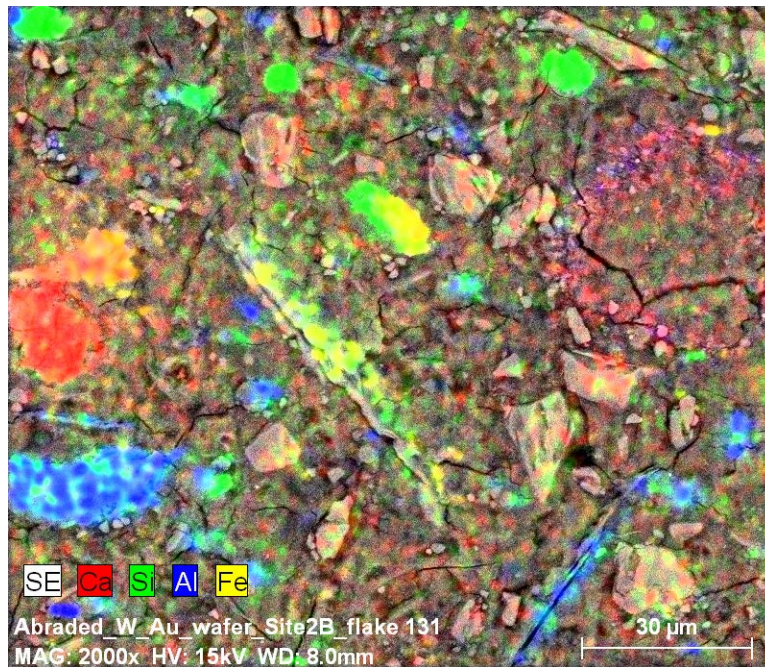


Figure 53. Elemental map of paste microstructure with Ca, Si, Al, and Fe noted in colors to aid in phase identification.



#### 8.4 Air Void Analysis

The entrained and entrapped air contents were 7.1% and 3.2%, respectively, for a total air content of approximately 10.3%. The spacing factor was 0.5 mm, higher than the 0.2 mm typically considered applicable for freeze/thaw resistance of concrete.

## 9 Summary and Conclusions

This study examined five concrete cores from the SDU6 facility at the DOE's SRS. The five cores, which were logged in as CMB No. 160051-1 to 05 were subjected to an in-depth analysis consisting of visual and petrographic examination, chemical spray indicator pH distribution, electron microscopy, elemental analysis, and hardened concrete air void analysis. The results of the study were:

- Overall, the concrete appeared to be of competent quality. Segregation was not observed nor the presence of large entrapped air voids or honeycombing.
- Cracks were observed in all cores received with the exception of Core Sample #2. When large cracks (i.e., greater than 100  $\mu\text{m}$ ) were observed, they generally extended through the full depth of the concrete slab.
- Crack sizes ranged from 0.1 mm to greater than 1 mm in width with crack width generally decreasing with depth into the concrete.
- No vertical displacement was observed between adjacent crack faces. All displacement of cracks appeared to be in the horizontal axis of the slab.
- Gravity feed epoxy repairs appeared to be successful in cores #1, #3, and #4. The large crack observed in core #5, although repaired with gravity-fed epoxy, did not appear to have any infilling of epoxy. If epoxy was observed within cracks, it generally penetrated multiple cm into the concrete with successful infilling of the crack with the exception of locations where the crack intersected large entrapped air voids. It is unclear whether these voids in the epoxy jeopardize water tightness except in cases where the cracks were fully infilled with no voids present.
- In many cases, cracks appeared to intersect and crack through coarse aggregates. Given the high quality granite used in the concrete at SDU6, cracking through the aggregates suggests a significant buildup of internal stress to generate cracks. Aggregate interfaces appeared

- tight even in the vicinity of cracks, suggesting a high strength and dense hydrated cement paste.
- Higher magnification optical microscopy and electron microscopy evidenced the anticipated microstructure based on the mixture proportion provided to the ERDC. The paste appeared to be very dense, with entrained air present meeting the required air content, and a greenish color indicative of a high slag content concrete.
  - pH indicator solution measurements made using optical microscopy indicated that the concrete at the surface had reduced pH to depths of approximately 1 to 2 mm. This reduction in pH did not extend down the interior of cracks. It is likely that discoloration at the surface of the concrete was caused by exposure to acidic water or natural carbonation processes while discoloration on the face of cracks is caused by oxidation of the slag rich paste in the concrete and minor impregnation of the faces of the crack with epoxy, if present.
  - High magnification electron microscopy evidenced anticipated phases with a large proportion of unhydrated / unreacted phases including spherical fly ash particles, angular unhydrated cement particles, angular unreacted slag particles, and hydrated cement paste. The presence of a significant amount of unhydrated / unreacted material was anticipated based on the high supplementary cementitious materials content in the concrete combined with a low water-to-cementitious materials ratio of less than 0.40. The paste microstructure was very dense with minimal porosity.
  - Distributed microcracking was observed throughout the paste with crack sizes of single to sub micrometer in size that was likely driven by shrinkage. This microcracking appeared to be fairly uniformly distributed throughout the depth of the concrete.
  - Elemental mapping performed also confirmed anticipated phases based on the mixture proportion and particle morphologies observed during SEM imaging.
  - Air void analysis measurements indicated that the concrete met air content requirements in all cases.

Based on the petrographic analysis presented herein and knowledge of the mixture proportion and construction procedures, the cracking observed in the concrete cores is likely associated with different forms of shrinkage. Small microcracks (less than 10-50  $\mu\text{m}$ ) in width in the near surface concrete are likely due to early-age crazing that occurred during finishing operations. These cracks appear to have largely self healed with mineral infilling. The larger through-depth cracks observed in cores #1, #3, #4, and #5 appear to be driven by internal shrinkage combined with restraint to that shrinkage from the base and connections along the perimeter of the slabs in the continuously reinforced concrete. These through depth cracks appear to have occurred later due to the fact that aggregate interfaces appear to be tight and well bonded with multiple cases where the crack actually fractured coarse aggregates. No vertical displacement was observed between adjacent crack faces. These cracks are likely passive in nature and no new cracks will form due to the concrete material itself. It may be possible for existing cracks to grow under excessive deformation and this should be monitored as the structure is loaded such as during a leak test.

Based on the mixture proportion and information on construction practices provided to the ERDC, it is possible that both drying and autogenous shrinkage played a role in the cracking. Drying shrinkage, a result of the evaporative loss of moisture, may occur as moist curing is removed from the surface of the concrete and water evaporates from the concrete. Autogenous shrinkage is also a likely driver for the observed shrinkage-induced cracking given the water-to-cementitious materials ratio of less than 0.40, high fines content, and high supplementary cementitious materials content in the concrete. Autogenous shrinkage will cause concrete to internally self desiccate, leading to shrinkage. This condition would be exacerbated by the use of curing compounds which seal off the concrete from being able to imbibe externally applied moisture during curing. Additional information regarding these forms of shrinkage in concrete and the applicability of curing compound in high-performance concrete can be found in:

- Kosmatka, Steven H., and William C. Panarese. Design and control of concrete mixtures. Vol. 5420. Skokie, IL: Portland Cement Association, 2002, pg 220.

- Aïtcin, Pierre-Claude. High performance concrete. CRC Press, 2011, pg 327.
- Report on High-Strength Concrete – ACI 363R-92. American Concrete Institute, 1997, pg 18.
- Guide to Curing Concrete – ACI 308R-5. American Concrete Institute, 2001, pg 5.

Another interest expressed to the ERDC by the SRS was the potential for self healing of cracks. It appears that high pH unhydrated material still exists in close proximity to internal cracks. Many of these cracks are less than 100  $\mu\text{m}$  in size and do have a potential for self healing if high pH water can be supplied to those cracks. However, many of these larger cracks have been sealed off by epoxy which may reduce the potential for self healing of cracks. In addition, it is likely that mere exposure to rain prior to placement of the roof structure would have already healed cracks in the concrete but this does not appear to have occurred. Additional studies in simulated saturated calcium hydroxide solutions may be used to study the potential for self healing of cracks to minimize leakage. This self healing will likely only result from reaction of unhydrated portland cement and residual latent hydraulic slag particles. It would take significantly higher solution pH levels (greater than 1 N to more than 10 N hydroxide solutions) to activate unreacted fly ash particles via geopolymerization reactions. Achieving these high pH levels to activate fly ash is likely impractical given the large volume of the SDU6 tank.

Overall, the concrete appears to be of high quality and contain the desired constituents that were mixed at the correct proportions per the project specifications. It appears that shrinkage, drying and autogenous, were the driving mechanisms for cracking. The results of this analysis should be compared with construction records related to curing and the occurrence of cracks to better identify the cause for cracking.

## **Contact Information**

For any questions related to the results of this study please contact:

Robert D. Moser, Ph.D.

Research Civil Engineer

Engineering Systems and Materials Division – Research Group

Geotechnical and Structural Laboratory

U.S. Army Engineer Research and Development Center

Phone: (601) 634-3261

Robert.D.Moser@usace.army.mil